AFRL-AFOSR-VA-TR-2015-0360

ADAPTIVE IR SENSING BASED ON ADVANCED NANOSTRUCTURES WITH TUNABLE KINETICS

Vladimir Mitin
RESEARCH FOUNDATION OF STATE UNIVERSITY OF NEW YORK THE

11/05/2015
Final Report

Air Force Research Laboratory
AF Office Of Scientific Research (AFOSR)/ RTA1
Arlington, Virginia 22203
Air Force Materiel Command

REPORT DOCUMENTATION PAGE

Form Approved
OMB No. 0704-0188

PLEASE DO NOT RETURN YOUR FORM TO THE ABOVE ORGANIZATION.

1. REPORT DATE *(DD-MM-YYYY)*	2. REPORT TYPE	3. DATES COVERED *(From - To)*
01-09-2015	Final	1 August 2010 - 31 July 2015

4. TITLE AND SUBTITLE
Adaptive IR Sensing Based on Advanced Nanostructures with Tunable Kinetics

5a. CONTRACT NUMBER
FA9550-10-1-0391

5b. GRANT NUMBER

5c. PROGRAM ELEMENT NUMBER

6. AUTHOR(S)
Mitin, Vladimir and Sergeev, Andrei

5d. PROJECT NUMBER

5e. TASK NUMBER

5f. WORK UNIT NUMBER

7. PERFORMING ORGANIZATION NAME(S) AND ADDRESS(ES)
University at Buffalo

8. PERFORMING ORGANIZATION REPORT NUMBER
account 1090223-1-55248

9. SPONSORING/MONITORING AGENCY NAME(S) AND ADDRESS(ES)
Research Foundation of the State University of New York
Sponsored Project Services
402 Crofts Hall
Buffalo NY 14260-0001

10. SPONSOR/MONITOR'S ACRONYM(S)

11. SPONSOR/MONITOR'S REPORT NUMBER(S)
account 1090223-1-55248

12. DISTRIBUTION/AVAILABILITY STATEMENT
Distribution A

13. SUPPLEMENTARY NOTES

14. ABSTRACT
The research program established scientific, engineering, and technological basis for further development of IR nanomaterials with nanoscale potential profile that can be effectively controlled by voltage bias and/or optical bias. While currently optoelectronic devices are based on the structures with potential barriers changing in one and/or two dimensions, the innovative approach is based on the novel paradigm of 3D nanoscale potential, which strongly enhances functionality of materials and structures. Moreover, bias-tunable nanoscale profile provides fast and efficient control of all optoelectronic properties of novel reconfigurable nanomaterials. Achieved tunable and sensing functionalities provide fast and effective control of the major optoelectronic properties including photocarrier lifetime, electron transport, spectral characteristics, noise parameters, and coupling to electromagnetic radiation.

We also demonstrated that the single graphene layer, graphene bi-layers, graphene nano-ribbon, and multiple graphene layer structures opens up prospects of further enhancement of capabilities of graphene-based optoelectronic devices, in particular, IR detectors and emitters.

15. SUBJECT TERMS
IR detectors, quantum dots, quantum wells, graphene, adaptive nanomaterials, IR emitter

16. SECURITY CLASSIFICATION OF:			17. LIMITATION OF ABSTRACT	18. NUMBER OF PAGES	19a. NAME OF RESPONSIBLE PERSON
a. REPORT	b. ABSTRACT	c. THIS PAGE			Vladimir Mitin
U	U	U	UU	44	19b. TELEPHONE NUMBER *(Include area code)* 716-645-1036

Reset

Standard Form 298 (Rev. 8/98)
Prescribed by ANSI Std. Z39.18
Adobe Professional 7.0

INSTRUCTIONS FOR COMPLETING SF 298

1. REPORT DATE. Full publication date, including day, month, if available. Must cite at least the year and be Year 2000 compliant, e.g. 30-06-1998; xx-06-1998; xx-xx-1998.

2. REPORT TYPE. State the type of report, such as final, technical, interim, memorandum, master's thesis, progress, quarterly, research, special, group study, etc.

3. DATES COVERED. Indicate the time during which the work was performed and the report was written, e.g., Jun 1997 - Jun 1998; 1-10 Jun 1996; May - Nov 1998; Nov 1998.

4. TITLE. Enter title and subtitle with volume number and part number, if applicable. On classified documents, enter the title classification in parentheses.

5a. CONTRACT NUMBER. Enter all contract numbers as they appear in the report, e.g. F33615-86-C-5169.

5b. GRANT NUMBER. Enter all grant numbers as they appear in the report, e.g. AFOSR-82-1234.

5c. PROGRAM ELEMENT NUMBER. Enter all program element numbers as they appear in the report, e.g. 61101A.

5d. PROJECT NUMBER. Enter all project numbers as they appear in the report, e.g. 1F665702D1257; ILIR.

5e. TASK NUMBER. Enter all task numbers as they appear in the report, e.g. 05; RF0330201; T4112.

5f. WORK UNIT NUMBER. Enter all work unit numbers as they appear in the report, e.g. 001; AFAPL30480105.

6. AUTHOR(S). Enter name(s) of person(s) responsible for writing the report, performing the research, or credited with the content of the report. The form of entry is the last name, first name, middle initial, and additional qualifiers separated by commas, e.g. Smith, Richard, J, Jr.

7. PERFORMING ORGANIZATION NAME(S) AND ADDRESS(ES). Self-explanatory.

8. PERFORMING ORGANIZATION REPORT NUMBER. Enter all unique alphanumeric report numbers assigned by the performing organization, e.g. BRL-1234; AFWL-TR-85-4017-Vol-21-PT-2.

9. SPONSORING/MONITORING AGENCY NAME(S) AND ADDRESS(ES). Enter the name and address of the organization(s) financially responsible for and monitoring the work.

10. SPONSOR/MONITOR'S ACRONYM(S). Enter, if available, e.g. BRL, ARDEC, NADC.

11. SPONSOR/MONITOR'S REPORT NUMBER(S). Enter report number as assigned by the sponsoring/ monitoring agency, if available, e.g. BRL-TR-829; -215.

12. DISTRIBUTION/AVAILABILITY STATEMENT. Use agency-mandated availability statements to indicate the public availability or distribution limitations of the report. If additional limitations/ restrictions or special markings are indicated, follow agency authorization procedures, e.g. RD/FRD, PROPIN, ITAR, etc. Include copyright information.

13. SUPPLEMENTARY NOTES. Enter information not included elsewhere such as: prepared in cooperation with; translation of; report supersedes; old edition number, etc.

14. ABSTRACT. A brief (approximately 200 words) factual summary of the most significant information.

15. SUBJECT TERMS. Key words or phrases identifying major concepts in the report.

16. SECURITY CLASSIFICATION. Enter security classification in accordance with security classification regulations, e.g. U, C, S, etc. If this form contains classified information, stamp classification level on the top and bottom of this page.

17. LIMITATION OF ABSTRACT. This block must be completed to assign a distribution limitation to the abstract. Enter UU (Unclassified Unlimited) or SAR (Same as Report). An entry in this block is necessary if the abstract is to be limited.

1. SUMMARY

A key challenge facing the modern IR sensing technologies is to provide the optimal use of the available but limited sensing resources to gather the most important data for target detection, tracking, classification, and identification. Currently the sensing process is mainly considered as a passive process, i.e. information gathered by the sensing resources undergoes analysis without any feedback to the sensor network and without sensor management. Adaptive sensor management has a strong potential for critical improvements in the efficiency of the sensor network by automatically controlling and coordinating main parameters of individual sensors simultaneously with processing resources.

The project addressed development of novel reconfigurable nanomaterials and adaptive IR detectors for third generation infrared imaging systems. The research program focused on design on advanced quantum dot (QD) and quantum well (QW) nanostructures and graphene-based nanomaterials with tunable kinetics of photoelectrons. The proposed work directly addressed the AFOSR needs in adaptive IR sensing, which is not available from any other current technological approaches.

The research program established scientific, engineering, and technological basis for further development of IR nanomaterials with nanoscale potential profile that can be effectively controlled by voltage bias and/or optical bias. While currently optoelectronic devices are based on the structures with potential barriers changing in one and/or two dimensions, the innovative approach is based on the novel paradigm of 3D nanoscale potential, which strongly enhances functionality of materials and structures. Moreover, bias-tunable nanoscale profile provides fast and efficient control of all optoelectronic properties of novel reconfigurable nanomaterials. In quantum dot nanomaterials the reconfigurable 3D nanoscale profiles is created by charged quantum dots or dot clusters selectively grown at special positions. Dots are charged to create repulsive potential so the photoexcited carriers are forced to move between the dots (rather than through the dots) and the probability for them to be captured back into dots substantially reduced. Selective bipolar doping allows us to obtained large potential barriers (barrier height is substantially larger than kT) even in structures with small electron filling of quantum dots and, therefore, with small dark current. Nanoscale engineering and tuning of electron processes is realized by manipulating the built-in-dot charge via voltage and optical biases. Long and manageable photoelectron lifetime is obtained by potential barriers that separate photoexcited electrons from QDs. Scalability of nanoblocks (QDs, QWs, and graphene-based materials) provides high flexibility of the proposed approach. The combination of theoretical analysis, numerical simulations of the electronic spectra, transport and relaxation, growth and processing technologies of semiconductor and graphene structures, and comprehensive analysis of the test structures and devices allowed the research team to identify the physical mechanisms of the interplay between tunable nanoscale potential and optoelectronic characteristics of IR nanomaterials. Achieved tunable and sensing functionalities provide fast and effective control of the major optoelectronic properties including photocarrier lifetime, electron transport, spectral characteristics, noise parameters, and coupling to electromagnetic radiation.

We also demonstrated that the single graphene layer, graphene bi-layers, graphene nano-ribbon, and multiple graphene layer structures opens up prospects of further enhancement of capabilities of graphene-based optoelectronic devices, in particular, IR detectors and emitters.

Besides DoD applications, the reconfigurable IR nanomaterials have a strong potential to address a number of other applications highlighted by the National Signature Initiative (NSI), especially the NSI Sensors Thrust.

2. INTRODUCTION

It is strongly expected that development of novel adaptable nanomaterials with manageable optical and kinetic properties leads to qualitatively new sensing technologies. Currently IR sensing is widely used in radar and imaging applications. Advanced systems for target detection, tracking, and identification require a multi-sensor platform with variety of sensors that have various spectral, dynamic, and noise characteristics. Development and implementation of sensors with adaptable parameters would provide optimal use of sensing resources and in this way enhance real-time detection and simultaneously decrease the cost of sensing system. Other numerous applications in global environmental, remote industrial and military monitoring, and homeland security are based on IR spectroscopy. Currently various types of spectrometers are used for various applications depending on their suitability for the spectral region of the particular application. Adaptive sensors would substantially increase the spectrometer bandwidth and critically enhance possibilities for precise identification of complex chemical agents. Offering novel materials, nanotechnology holds intriguing promises for enhancement of IR sensing technologies in the nearest future. Rapid improvements in the synthesis and processing of novel nanomaterials open up new opportunities for fabrication of nanomaterials and nanostructures with adjustable parameters for intelligent sensing. Numerous imaging applications include such large market segments as security, driving, and navigation. IR spectroscopy is also used in global environmental and industrial monitoring as well as in homeland security. All above applications will strongly benefit from the development of adaptive sensors based on adaptable nanomaterials. Even relatively simple firefighting IR camera should have large dynamic range to detect targets at varying background temperature. Adaptable nanomaterials are expected to demonstrate wide spectral tunability, adjustable dynamic range for detection of high and low intensity radiation, possibilities to operate at high level background radiation, scalability to use in large sensor arrays for imaging application, light weight and low power consumption, radiation hardness, and, finally, manageable trade-off characteristics, such as operating time and sensitivity (noise equivalent power, detectivity) in the direct detection and bandwidth and local oscillator power in the heterodyne detection.

Currently the sensing process is mainly considered as a passive process, i.e. information gathered by the sensing resources undergoes analysis without any feedback to the sensor network and without sensor management. There is no provision for adjusting the sensing process for achieving optimal combination of the sensitivity and acquisition time to meet mission requirements. Variety of operating regimes of an individual sensor and adjustable dynamic range due to these regimes form a basis for the hierarchical adaptive architecture. Adaptivity of a sensor assumes possibilities for wide range changes in sensors parameters. Long operating time increases responsivity and improves noise characteristics. Sacrificing the sensitivity, one can significantly increase the operating speed, i.e. decrease the acquisition time. High scalability of the sensors together with advanced multiplexing allow for highly manageable fusion and processing architecture with sufficient autonomy of each node.

Sensor management is a key point for adaptive data fusion. It directs sensing resources in an adaptive way to acquire data that is the most relevant to the mission objectives in accordance with their hierarchical structure. For example, a task such as identification and tracking an enemy platform has a higher priority than performing a general survey. Then the platform identification will require high sensitivity, while the tracking of a maneuvering target needs fast operating speed. The management module will develop sensing priorities taking into account the current

analysis of a situation and previous data about the platform. Coordinated sensor management will provide control of limited sensing resources and will allow for collecting the most critical information about the platform and its motion.

In Table I, we summarize the desirable characteristics of the data fusion and processing together with sensor requirements, which should be addressed to achieve these characteristics.

Table I. Sensor requirements for adaptive data fusion and processing

Data Fusion and Processing	**Sensor Requirements**
Hierarchical architecture with dynamic links	Variety of operating regimes High dynamic range of an individual sensor
Flexibility and adaptivity	Wide range flexibility of the trade-off parameters, such as responsivity, sensitivity, and operating time
Tunability to the current situation	High tunability of spectral and noise characteristics
Manageable architecture Sufficient autonomy of each node	High scalability of sensors Advanced multiplexing

Advances in nanotechnology lead to new fascinating possibilities to fabricate nanomaterials, which combines various combinations of quantum dots (QDs), QD planes, rows, clusters, quantum wells (QW), quantum dot in wells, and graphene (GRP) based nanostructures. These nanomaterials open wide possibilities for nanoscale engineering of optic and electric processes. In our opinion, the most effective and reliable way to manage photocarrier characteristics is to control the electric charge of nanoblocks, such as quantum dots and quantum wells. Numerous potential applications of nano-inspired sensing materials are highlighted by the NSI Sensors Thrust of National Signature Initiative (NSI). Substantial achievements have been reached in enhancing the sensor functionality and spectral tunability due to nanoscale band engineering. However, despite intense research efforts, the progress in development of reconfigurable sensing materials is still very limited.

This project focused on design of adaptive infrared (IR) detectors based on advanced nanostructures with tunable kinetics of photoelectrons. The program directly addressed the AFOSR needs in adaptive IR sensing (Fig. 1).

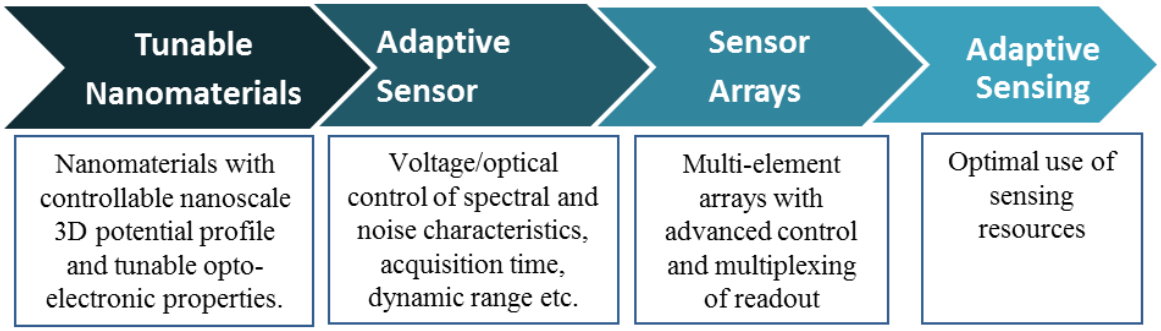

Figure 1. Multi-level integration from electrically/optically tunable nanomaterials to adaptive multi-sensor arrays.

The primary goal was to develop nanostructures with tunable optoelectronic characteristics, which can be managed in wide ranges that required by adaptive sensing.

Our original approach is based on nanostructures (QD, QW, and GRP structures) with a electrically/optically-tunable 3D nanoscale profile . The 3D nanoscale profile is essentially a new paradigm in optoelectronic devices. Typically, the operation of semiconductor structures is solely based on a bias and/or gate control of microscale potential profile, which is managed in one or two directions. Selective and compensated doping will allow us to obtain large potential barriers (eV >> kT) around dots even in materials with small electron number of carriers in QDs. Nanoscale engineering and tuning of electronic processes will be realized by manipulating the charge of QDs and QWs via voltage and optical biases. Long and manageable photoelectron lifetime will be obtained by forming potential barriers that separate photoexcited electrons from QDs and QWs. High flexibility of this approach (scalability of nanoblocks, manageable potential barriers etc.) provides high functionality of the nanomaterial.

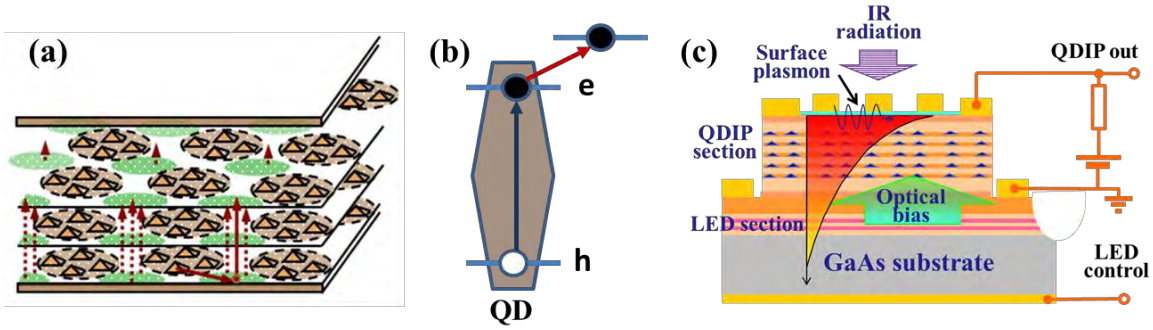

Figure 2. Integration of (a) functional nanoblocks via 3D nanoscale potential with (b) "optically biased" QDs into advanced optoelectronic nanomaterials and devices. (c) A concept tunable pixel design with optical biasing and near-field palsmonic enhancement of IR absorption.

The main idea of the reconfigurable QD nanomaterial and the optical control are shown in **Fig. 2**. As it is shown in **Fig. 2a**, the negatively charged dot clusters create significant potential barriers around clusters. The nanoscale potential barriers around QD clusters prevent photoelectron capture by QDs or by defects near QDs. Correlated positions of QDs form high mobility conducting channels that provide effective collection of photoelectrons. **Fig. 2b** illustrates the effect of the "optical bias". First, the optical radiation creates electron-hole pairs in QDs. Then the electrons are excited by IR radiation from the localized states in QDs to the conducting states in the matrix, where they contribute to the photocurrent. Without compensation doping the holes in the dot would attract photoelectrons and enhances the photoelectron capture. In the proposed structures with compensation doping, the negatively charged acceptors in QDs create potential barriers that drastically suppress the capture processes and provide long photoelectron lifetime and large optical gain. Optical bias of nanodevices gives a fast and effective way to manipulate with the electron filling of QDs.

The research program demonstrated feasibility of reconfigurable IR nanomaterials with the electrically/optically tuning of sensing characteristics. The developed materials have the following features that open wide perspectives for scalable integration them into advance sensing technologies:

- Manageable photoelectron kinetics, which allows for tuning the photocarrier lifetime to control basic sensor characteristics, such as response time, responsivity, and detectivity;
- Tunable highly-selective coupling to electromagnetic radiation due to control of QD levels and their occupations;
- High photoconductive gain and responsivity;
- High mobility of carriers and low dissipation;
- Controllable generation-recombination (GR) noise;
- High scalability of nanoblocks and numerous possibilities for nanoengineering;
- Compatibility with plasmonics technologies;
- Available fabrication technologies compatible with mainstream III-V compound semiconductor manufacturing.

3. METHODS, ASSUMPTIONS, AND PROCEDURES

3.1. Nanoscale engineering and tuning of electron processes by charging of QDs

Operation of all electronic and optoelectronic semiconductor devices is essentially based on bias and/or gate control of potential barriers for electrons and holes. Three-dimensional (3D) potential profiles can provide more functionality and scalability to optoelectronic materials and structures. Manageable nanoscale potential barriers are an effective tool for engineering of electron processes, which control electric and optical properties of nanomaterials. Tuning of the barriers by bias/gate voltage opens wide perspectives for the development of adaptable optoelectronic nanomaterials.

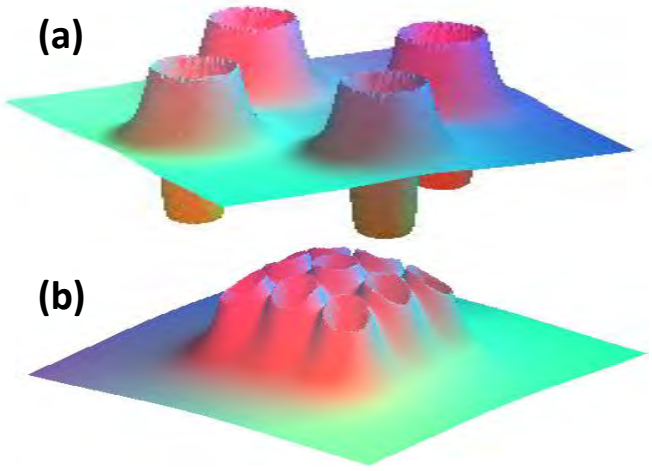

Figure 3. Potential barriers created by charged spherical quantum dots and dopants outside dots: (a) the barriers around single dots; (b) the collective barriers around a dot cluster with nine dots.

Charged quantum dots provide unique possibilities for creation of specific 3D potential profiles favorable for photovoltaic and sensing applications. Potential barriers around QDs are always formed when electrons from dopants outside QDs fill the dots. In the simplest case, uniformly distributed charged QDs create local potential barriers (**Fig. 3a**). Charged quantum dots with correlated positions, such as QD clusters, planes, rows etc. may be used to create higher

collective potential barriers (**Fig. 3b)** which separate the groups of QDs from conducting channels.

For effective engineering and tuning of electron processes, the potential barrier around QD should be 2-3 times larger than the thermal energy, $k_B T$. Therefore, at room temperature, the local barriers should be ~ 0.05 eV. To evaluate and illustrate the potential created by a single dot, in **Fig. 4** we present the electric potential of the half-filled spherical InAs quantum dot in GaAs matrix as a function of a QD radius, R.

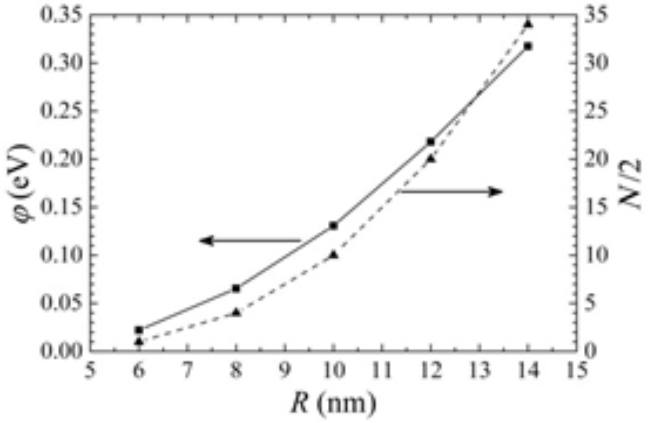

Figure 4. Height of potential barriers around the half-filled spherical GaAs QD.

As seen from Fig. 4, for spherical dots, even a QD charge of ~3 electrons per dot provides potential barriers effective for engineering and tuning of electron processes.

In reconfigurable IR nanomaterials the photo-absorption areas (QD nanoblocks, such as planes, rows, clusters) are separated from the areas transmitting the photocurrent (heterointerfaces and QWs) by potential barriers, which are created by charged dots and dopants. In other words, these barriers separate the localized electron states in the QDs from the high-mobility conducting electron states. **Figure 5** shows examples of such nanomaterials.

In nanomaterial with the lateral current along the heterointerfaces (**Fig. 5a**) the potential barriers are formed by charged QD planes and charged planes of dopants. The potential barriers separating QD planes from the conducting channels are determined by the charge of QD planes. Under weak radiation the charge of QDs, in turn, is mainly determined by doping of barriers between QD planes. The corresponding band structure is shown in **Fig. 5b.** management of barriers may be implemented via the gate potential. Gate control allows fast and effective tuning of both population of electron states in QDs and kinetics of photoelectrons.

Figure 5c shows a nanomaterial with vertically correlated dot clusters. Here, the barriers are created by charged dot clusters and dopants. Once the electrons are excited by the radiation, electrons drift in the areas between dot clusters. If the radius of the cluster, b, exceeds the distance between dot planes, c, a height of the potential barrier weakly (logarithmically) depends on in-plane geometry, i.e. $V_m \sim \ln(w/b)$, where $2w$ is the distance between the centres of two neighboring clusters. In this design, the barrier height is proportional to the electric charge of the cluster (**Fig. 5d)**. The charge can be controlled by the bias voltage.

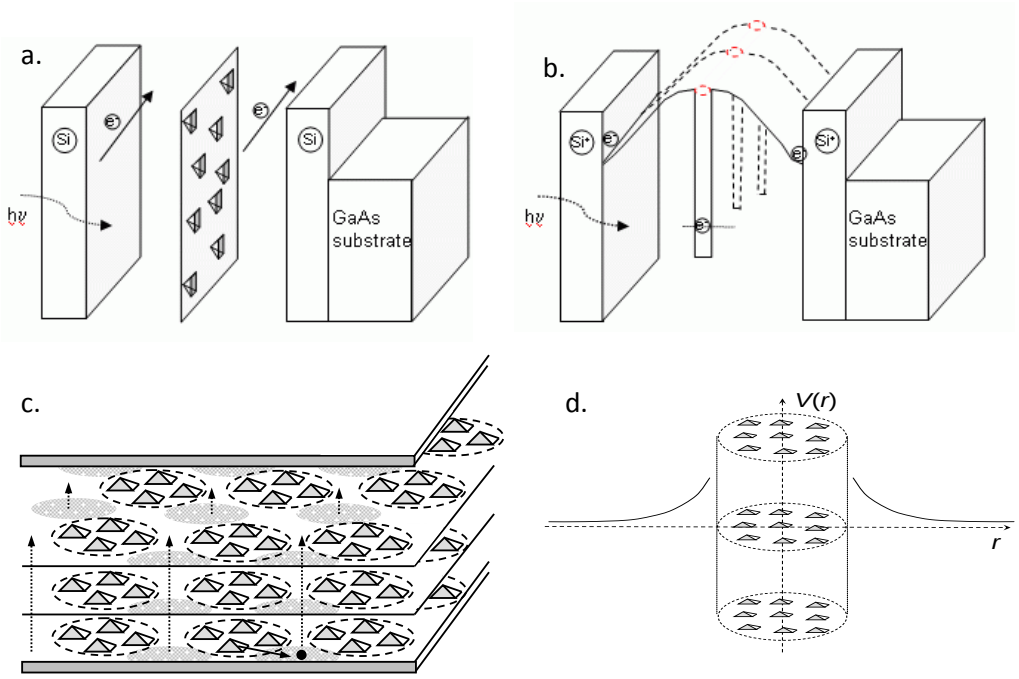

Figure 5. Examples of adaptable nanomaterials. (a) QD nanomaterial with lateral transport along QD planes and (b) corresponding band structure with barriers around QD planes; (c) nanomaterial with vertical photoelectron transport between vertically correlated QD clusters; (d) logarithmic potential barriers around vertically correlated QD clusters.

More strong separation of localized and high mobility states can be reached in the material, which combines QDs and QWs. An example of such material is presented in **Fig. 6**. In this nanomaterial with the lateral transport, the photoelectrons excited from QDs are captured by QWs and move over high mobility QWs to the contacts.

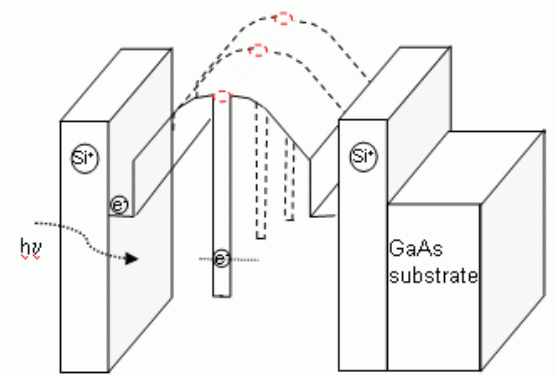

Figure 6. Nanomaterial, which combines QD planes with QWs. Photoelectrons excited from dots moves over QWs (lateral transport).

Thus, in adaptable nanomaterials, the barriers are controlled by the dot occupation, which in turn is determined by the doping and may be managed by the bias voltage and/or by additional gate.

3.2. Nanoscale modeling of electron processes and IR detectors

To describe electrical and IR properties of nanomaterials with built-in charge we have developed original theoretical models and simulation tools. The models and software were used to optimize the IR absorption, minimize recombination losses, and enhance tunability of IR nanomaterials. The general scheme of such optimization for nanostructures with Quantum Dots with Build In Charge (Q-BIC) is shown in **Fig. 7**. Optimization of QD media includes addition of capping layers to control size and shape of QDs and to reduce wetting layer (WL), adjustment of barriers via modulation bipolar doping, and tuning of inter-plane distance to optimize correlated positions of quantum dots.

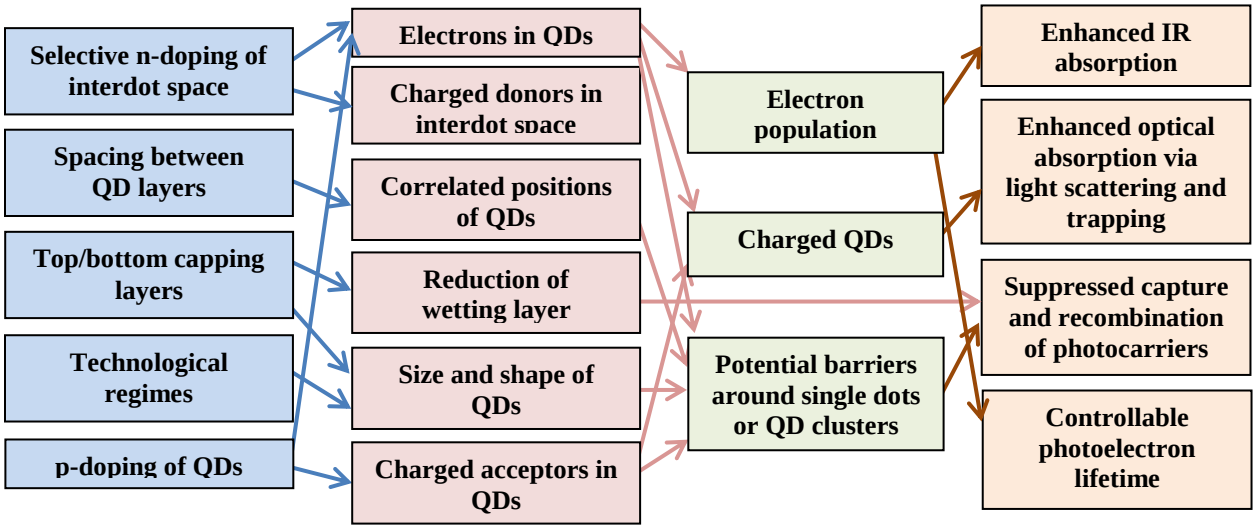

Figure 7. Complex integration and optimization of Q-BIC media: charged QDs provide effective control of electric and optical properties of nanomaterials via nanoscale potential profile.

To calculate the built-in-dot charge and investigate the potential profiles around dots, we used the nextnano3 software, which allows for simulation of multilayer structures combined with different materials of realistic geometries in one, two, and three spatial dimensions /http://www.nextnano.de/nextnano3/. This simulation tool self-consistently solves Schrödinger, Poisson, and current equations for electrons and holes. The conduction and valence bands of the structures are defined within a single-band or multi-band k·p model, which includes a strain.

The three-dimensional [3-D] potential profile in QD structures calculated with nextnano3 is shown in **Fig. 8**. The light black lines denote the preferable channels for the motion of photoelectrons (white dots) in the 3D nanoscale potential profile created by the built-in-dot charge. We simulated the band structure and potential distribution in real devices taking into account the effects of contacts. **Figure 9** shows variations of the built-in-dot charge and potential profile in the C-D cross section for the device with inter-dot doping of ten QD layers). As seen, the effect of contacts is important only for one or two QD layers adjacent to the contacts. Thus, the built-in-dot charge in QD layers from the third to the eighth is directly determined by the inter-dot doping.

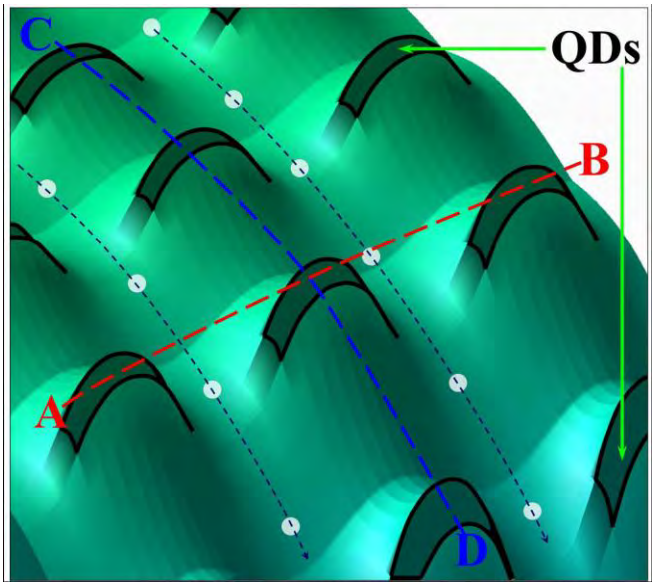

Figure 8. 3-D nanoscale profile of potential barriers around dots with built-in charge. A-B cross section is along the QD plane, and C-D cross section is in the direction of the vertical electron transport.

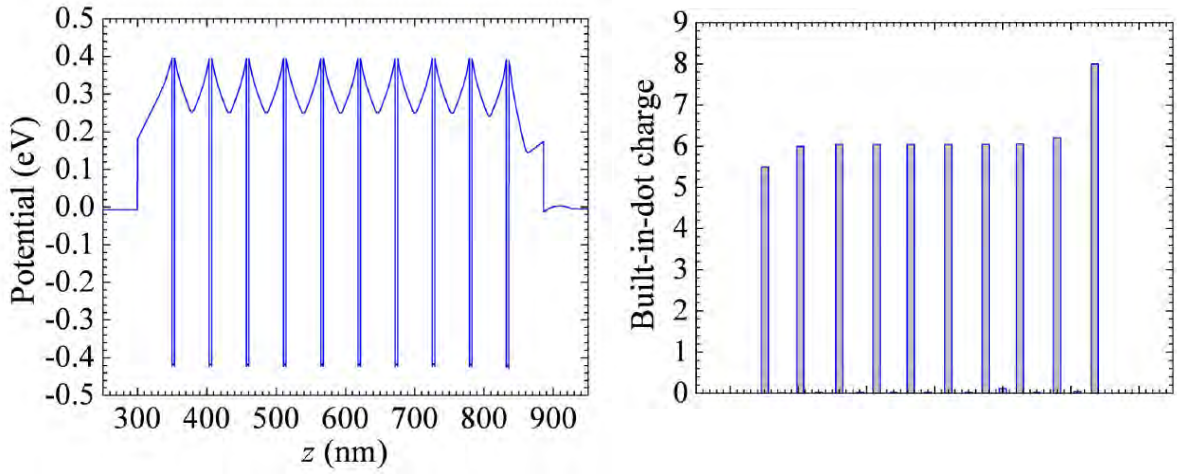

Figure 9. Potential distribution and built-in-dot charge along C-D cross section (see Fig. 8) over the device with ten QD layers and inter-dot doping.

The nanoscale potential profile is very sensitive to the shape of QDs. As it is shown in **Fig. 8**, the potential barriers in traditional structures with wetting layers are strongly anisotropic. The barriers in the QD planes, i.e. in the direction perpendicular to the current, are approximately one order of magnitude smaller than the barriers in the direction of the current. Reduction of wetting layer decreases the QD base, and increases its height. In **Fig. 10** we compare potential barriers in structures with and without wetting layers. As seen, at the same charge of a QD the form and height of the potential barrier substantially depends on the form of a QD. This shape modification drastically suppresses the capture processes.

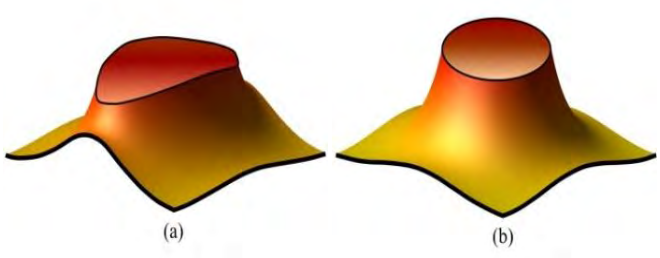

Figure 10. Potential barriers around QDs with (a) elliptic base a = 24 nm, b = 12 nm, and height h = 4 nm; and (b) circular base $a = b$ =14 nm and height h = 6 nm.

To study photoelectron kinetics in IR nanostructures we combine the nextnano3 software with our original Monte Carlo program, which includes all basic scattering processes, such as electron scattering on acoustic, polar optical, and intervalley phonons and electrons in Γ-, L-, and X-valleys.

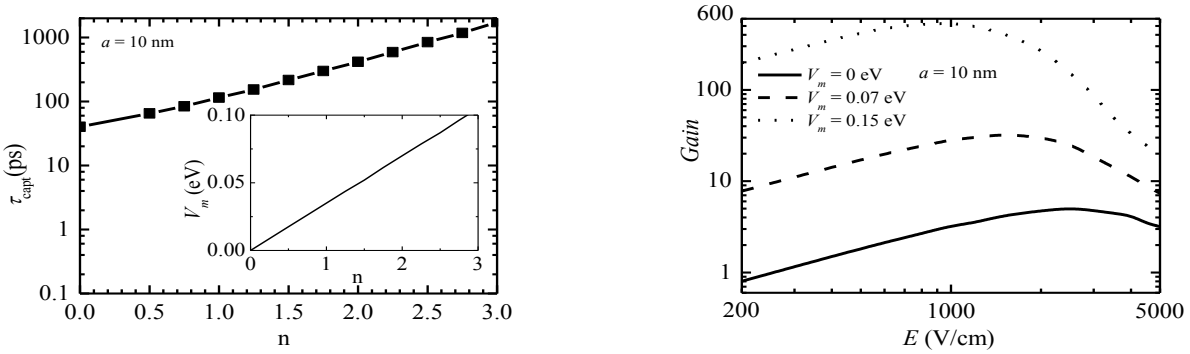

Figure 11. Results of Monte-Carlo modeling of photoelectron processes of vertically correlated QD structures (see Fig. 5c). (a) Capture time and the barrier height (insert) vs. number of electrons in per dot that defines the built-in-dot charge. (b) Photoconductive gain vs. the electric field.

Figure 11 shows results of modeling of photoelectron kinetics in the structures with collective potential barriers. In structures with vertically correlated positions of quantum dots (**Figs. 5c** and **5d**), positions of quantum dot clusters are correlated in the vertical direction and the photocarriers move in the areas between QD clusters through high-mobility conducting channels. **Fig. 11a** illustrates the exponential dependence of the capture time on the built-in dot charge for 9 dots in the cluster, and b= 75 nm, and w = 150 nm. **Fig. 11b** presents the photoconductive gain as a function of the electric field.

The advanced modeling demonstrate strong dependence of electric and IR properties of Q-BIC media on manageable nanoscale barriers on and charge redistribution between nanoscale blocks induced by the bias/gate voltage and optical bias. Reconfigurable nanomaterials allows for managing of the operation regimes due to strong dependences of the responsivity, photoelectron lifetime, spectra, and noise on the 3D nanoscale potential. **Figure 12** shows the scheme of tuning

of the photodetector characteristics via electric and optical control of the nanoscale potential profile.

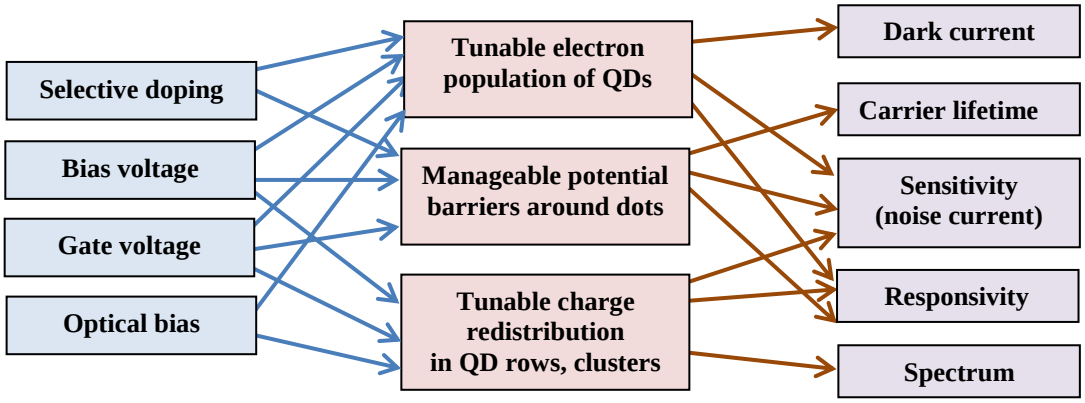

Figure 12. Integration and optimization of adaptive Q-BIC IR sensors: effective control of the photoelectron lifetime and electron population of QDs via bias/gate voltage and/or optical pumping.

3.3. Growth and selective doping of QD and QW structures

High scalability of nanoblocks provides numerous possibilities to create specific configurations of charged dots by selective doping. This leads to high tunability of QD spectral characteristics and electron characteristics of the QD media. In the investigated QD structures the thickness of the GaAs spacer layer between QD planes varis from 10 to 50 nm. The spacer thickness of 10 nm allowed us to fabricate QD planes with correlated position of QDs. The spacer thickness of 50 nm provides dissipation of strain fields in subsequent layers and reduction of strain accumulation in the multi-stack samples. To obtain correlated positions of QDs and, at the same time, to avoid stress accumulation, we fabricated structures with modulated spacer layer. **Fig. 13** shows an example of such structure, where three subsequent layers are separated by 10 nm GaAs barriers and these three-layer blocks are separated by 50 nm GaAs spacer. In the nanomaterials with charged QDs, the barriers around dots or groups of QDs are controlled by the dot occupation, which may be managed by the bias voltage.

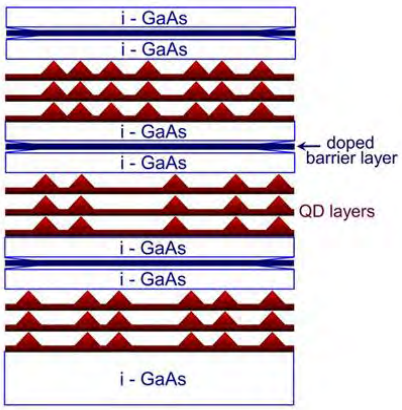

Figure 13. QD medium with partially correlated positions of QDs. Modulation of the spacer thickness dissipates the stress accumulation.

Quantum dot structures were grown using EPI GEN II MBE system equipped with elementary group III SUMO sources and As_2 beam generated from a valved cracker source. Ten – twenty QD layers were either randomly distributed over the thickness of 0.5 μm $Al_{0.22}Ga_{0.78}As$ barriers, or grouped in close spaced packs with interlayer distances around 20 nm. Silicon was used for doping of contact layers to the structure and for modulation doping of QDs into the barriers to create electron population within the QDs. Substrate temperature was typically kept constant for the entire QD- containing layer. InAs QDs were formed via Stranski-Krastanov process where InAs layer with 6.06Å lattice constant is nucleating as 3D islands over about monolayer-thick wetting layer on AlGaAs surface with lattice constant 5.65Å (7% biaxial strain). Formation of QDs critically depends on growth parameters, such as substrate temperature and arsenic overpressure, as well as total thickness of deposited InAs. Optimization of QD stack was performed using photoluminescence (PL) and secondary electron microscopy (SEM) as metrological techniques. For the SEM analysis, an incomplete QDIP structure with growth termination after completion of a certain (usually the third) QD layer was capped by 2 monolayers of AlAs to prevent the structure against further evolution and enable QD imaging using a top-view SEM.

For device fabrication, the top Ohmic contact was deposited using e-beam evaporation and lift-off of AZ 5214 image reversible photoresist. Since devices are expected to operate at low current densities, Cr-Au non-alloyed contact with relatively high series resistance was employed. Device mesa was patterned using thicker SPR220 resist and ICP etching in Cl2:BCl3: Ar plasma. Backside contact to n-type GaAs substrate was either e-beam deposited AuGe based contact or Indium.

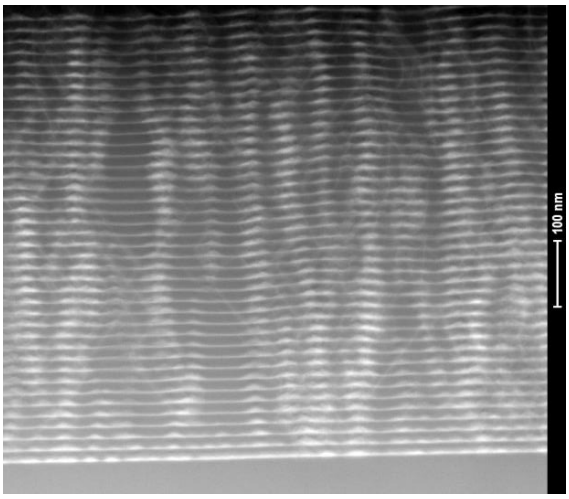

Figure 14. TEM of 40xQD sample. Dislocations can be seen propagating through the sample.

As discussed above, clustering of QDs may be used to increase interaction of photoelectrons with electrons localized inside clusters of adjacent QDs. TEM image in **Fig. 14** shows a cross-sectional view of a structure with 40 layers of densely packed QDs. The vertical stacking of QDs can be clearly seen in micrograph. Brighter lines which are seen in the image are dislocations arising from the strong lattice mismatch stress generated by a large amount of InAs in the structure. The dislocation density can be estimated as about 10^9 cm^{-2}. Dislocations at such concentration are expected to affect carrier lifetime, as well as doping efficiency.

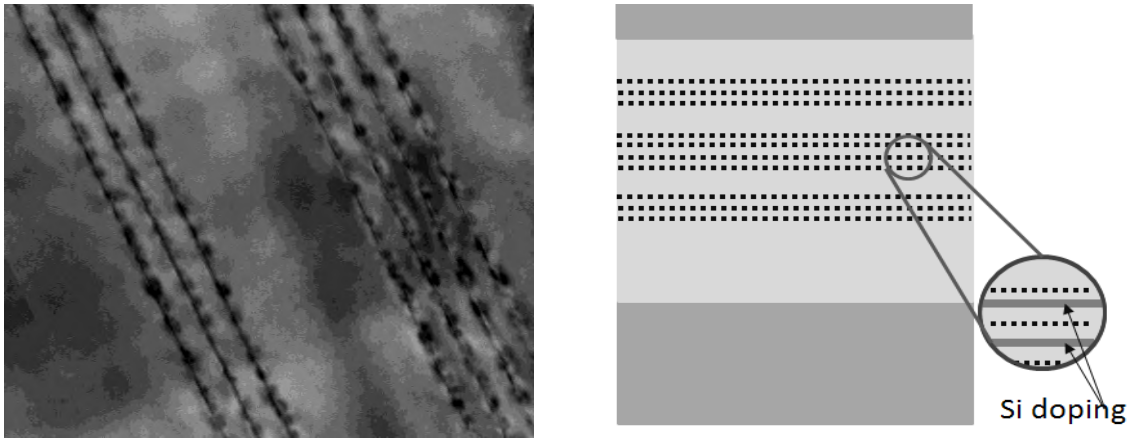

Figure 15. (a) TEM image and (b) schematic drawing of a structure with clustered groups of QD sheets. No dislocations are seen in TEM image, confirming significant improvement in structure quality compared to structures with high number of uniformly spaced QD layers.

To reduce the defect density in the QDIP absorber, we have employed another approach, when the same number of QD sheets is distributed in a different way within the thickness of i-region.

Devices having 10 layers with 50 nm spacing between the layers were compared with those where three groups of 3 or 4 layers separated by 20 or 25 nm are spaced by larger gaps as it is shown in **Fig. 15a.** As can be seen in the cross-sectional TEM image in **Fig. 15a** and schematically shown in **Fig. 15b**, these structures demonstrate much lower dislocation density compared to the previously discussed densely packed structures.

We also investigate effect of charging and charge redistribution in asymmetrically doped double-quantum-well (DQW). For these investigations the DQW structures were grown on a semi-insulating GaAs wafer to permit back side illumination.

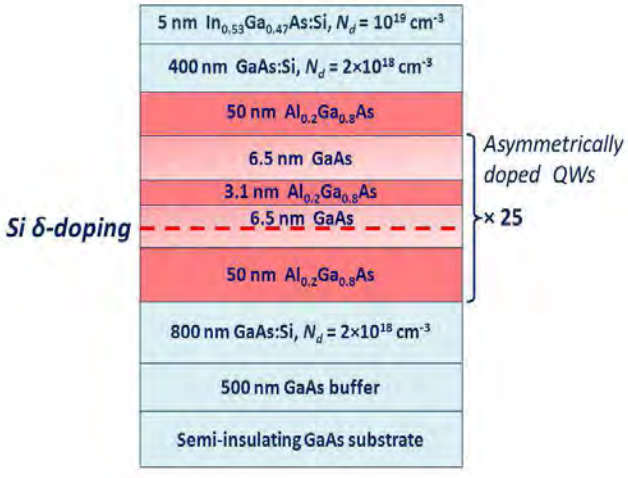

Figure 16. The DQW structure with asymmetric doping.

The growth sequence started with a 500 nm undoped GaAs buffer layer, and was followed by a 800 nm heavily doped ($N_d = 2 \times 10^{18}$ cm^{-3}) GaAs contact layer, 25 stages of the detection unit, 400 nm layer of GaAs doped to 2×10^{18} cm^{-3} as a contact layer, and finally 5 nm InGaAs layer doped to 10^{19} cm^{-3}. One unit of the structure is composed of 6.5 nm GaAs layer doped with Si with sheet density 5×10^{11} cm^{-2} and 6.5 nm undoped GaAs separated by 3.1 nm-thick $Al_{0.2}Ga_{0.8}As$. Each unit is separated by 50 nm $Al_{0.2}Ga_{0.8}As$ barriers (see **Fig. 11**). The growth was interrupted for 5 sec after GaAs growth for the sharp interfaces. The substrate was rotated continuously at a speed of 30 rpm. In-situ growth calibration growth rate for GaAs and AlGaAs layers, and Al concentration, was done by RHEED system and the layer thicknesses and Al mole fraction are confirmed by an X-ray diffraction (XRD) measurement after growth. The growth rates of GaAs and AlGaAs, Al mole fraction were measured 0.78 ML/s, 0.98 ML/s, and 20 %, respectively by RHEED. XRD revealed that the layer thicknesses are 4% thicker than the nominal values. The Quantum Well Infrared Photodetector (QWIP) was processed by standard photolithography, wet chemical etching, and metallization techniques. The first lithography step was performed for defining mesa structure. The mesa structures of 100×100 μm^2 and 200×100 μm^2 were defined with sulfuric acid ($H_2SO_4 : H_2O_2 : H_2O = 10 : 10 : 300$) which provides an etch rate of 0.155 μm/min. The etch rate was calibrated by atomic force microscope. The second lithography was performed for the metal deposition. Prior to the deposition, native oxide layer was removed by ammonium hydroxide solution ($NH_4OH:H_2O = 10 : 300$). Contacts, Ni/Ge/Au/Ni/Au layers with thicknesses of 2/14/28/40/100 nm, respectively, were deposited by Edwards e-beam evaporator. The metal contacts were deposited on the heavily Si doped GaAs contact layers and followed by rapid thermal annealing in N_2 ambient for 40 sec at 430 °C to form ohmic contact with the device resistance of ~ 30 Ω.

Summarizing this section we would like to highlight that our original approaches essentially combine the nanoscale band engineering with engineering of the nanoscale potential profile. Formation of nanoscale barriers due to modulation doping drastically enhance functionality of nanosctructures for use in advanced sensing technologies.

4. Results and Discussion

4.1. Photoelectron Kinetics in Nanoscale Potential Profile: Model Development

Our novel approach is based on managing of photocarrier kinetics by managing 3D nanoscale potential profile. Here we consider profiles created by charged QDs. Dot charging is realized via selective doping of the interdot space. Potential barriers around QDs are always created, when electrons from dopants outside QDs fill the dots. It is well-understood that the QDs are effective centers of recombination. Therefore, suppression of photoelectron capture into QDs directly increases the photoelectron lifetime and decreases the recombination losses. To suppress the photocarrier capture by potential barriers, the barrier height should be two-three times larger than $k_B T$. Therefore, at room temperatures, the local barriers should be ~ 0.05 eV and QDs should comprise 5-10 electrons. This requires relatively large dots and relatively high level of doping. Manipulations with QD clusters provide numerous possibilities for creating of high potential barriers with specific shapes that are favorable for optoelectronic and photovoltaic applications. Another approach employs the bipolar doping that allows one to create large potential barriers around dots with small electron filling.

Complex structure of the electron energy levels in nanomaterials is critically important for engineering of photoelectron kinetics. The huge difference between electron and hole processes are mainly determined by structures of electron and hole energy levels. The level structure in InAs/GaAs quantum dots has been investigated in numerous photoluminescence measurements. All data show practically equidistant level positions of electrons and holes, as shown in **Fig. 17**. The total level spacing, $\Delta E = \Delta E_e + \Delta E_h$, which was directly determined in our photoluminescence experiments and found to be 60 – 80 meV. The specific equidistant positions of energy levels may be associated with the quasi-parabolic form of the confinement potential in InAs/GaAs QDs. In this model, the spacing ratio, $\Delta E_e/\Delta E_h$, is given by $(m_h/m_e)^{1/2} \approx 4$, which is in agreement with the scope of various experimental results. Using this model we get: $\Delta E_e \approx 50$ - 65 meV and $\Delta E_h \approx 10$ -16 meV. Other groups reported data close to ours. Thus, for IR detection one should choose the IR-induced electron transition.

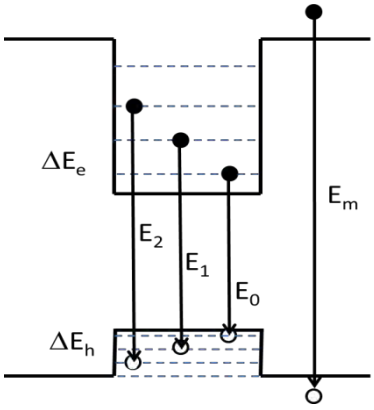

Figure 17. Level structure in InAs/GaAs quantum dots. The total level spacing $\Delta E = \Delta E_e + \Delta E_h = 60 – 80$ meV; the electron level spacing is substantially larger than that for holes: $\Delta E_e / \Delta E_h \sim 4$.

The photoelectron capture by the repulsive charged QD may be realized via *tunneling* through the barrier or *thermal excitation* above the barrier. Let us first evaluate the relative probability of these two processes for a simple model of spherical dot of radius a. The probability of the tunneling reaches a maximum for electron moving along the dot radius.

For electron with energy ε, this probability is proportional to $\exp[-2\pi(E_B/\varepsilon)^{1/2}]$, where E_B is the Bohr energy, $E_B = 2\pi^2 N^2 e^4 m/h^2\kappa$, where N is the number of electrons captured in a dot, m is the electron mass, and κ is the permittivity. Then, in the case of the Boltzmann distribution of photocarriers, the tunneling probability is proportional to $\exp[-2\pi(E_B/\varepsilon)^{1/2} - \varepsilon/k_BT]$. The characteristic energy of tunneling particles is given by $\varepsilon^* = [E_B (\pi k_B T)^2]^{1/3}$. The characteristic spatial scale is determined by the turning point for the tunneling under the Coulomb barrier: $r^* = Ne^2/(\kappa\varepsilon^*)$. For the electron with the energy ε^* we have

$$r^* = \left[\frac{2N}{\pi^2 \kappa} \frac{\hbar^2}{e^2 m} \left(\frac{e^2}{k_B T} \right)^2 \right]^{1/3} . \qquad (1)$$

Evaluating Eq. (1) for $N \sim 5$, we get $r^* \sim 5$ nm at a room temperature. If characteristic dot size, *a,* is smaller than r^*, the tunneling processes dominate in the photoelectron capture. In this case, the temperature dependence of the capture rate is expected to be the same as for the repulsive impurity centers,

$$\frac{1}{\tau_{capt}} \propto \exp\left[-\left(\frac{27\pi^2 E_B}{k_B T}\right)^{1/3}\right]. \tag{2}$$

In the opposite case, $r^* <> a$, the thermal activated processes dominate over tunneling and the electron capture rate is expected to follow to the exponential dependence

$$\frac{1}{\tau_{capt}} = \pi N_d a^3 \tau_\varepsilon^{-1} \exp\left[-\frac{Ne^2}{k_B T \kappa a}\right], \tag{3}$$

where N_d is the dot concentration, τ_ε is the inelastic scattering time, which corresponds to transitions with characteristic QD spacing due to electron interaction with optical phonons. Usually in QD structures the characteristic dot size is comparable or larger than r^*. Therefore, in contrast to the capture by the repulsive impurity centers, the capture rate by charged QDs exponentially depends on the height of potential barriers.

Nanoscale barrier induced suppression of the photoelectron capture improves the photoconductive gain, which is defined as:

$$g = \tau_{capt} / \tau_{tr}, \tag{4}$$

where τ_{tr} is the electron transit time, i.e. the time that an electron spends in the detector moving from the emitter to the collector. Increase of the gain does increases the responsivity, which is directly proportional to the gain. High responsivity provides an easy matching of the device to the readout and decreases the noise of the readout amplifier in the complete system.

4.2. Nanoscale Engineering of Potential Barriers

InAs/GaAs QD structures are typically grown epitaxially in Stranski-Krastanow growth mode that results in significant volume of the wetting layers in structure. The most efficient electron capture pathway begins with the capture of photoelectron into the wetting layer (WL). As it is shown in **Fig. 18**, the WL is geometrically overlapped with QDs and, therefore, the electron transition from WL to QDs is very efficient. As a result, the electron capture time to the uncharged QDs turns out to be in the subpicosecond range.

To further suppress recombination processes in Q-BIC devices we fabricated and investigated structures with reduced wetting layer.

In order to reduce the WL we grow the nanometer $Al_{0.2}Ga_{0.8}As$ bottom ayer, on which we grow InAs quantum dots. QD growth occurred following the deposition of 2.1 MLs of InAs on $Al_{0.2}Ga_{0.8}As$ bottom layer. After that the top nanometer $Al_{0.2}Ga_{0.8}As$ layer was deposited to further reduce the WL. Because of the high InAs/AlGaAs interface energy, the formation of InAs QD between two AlGaAs layers radically reduces the InAs wetting layer, almost eliminating it.

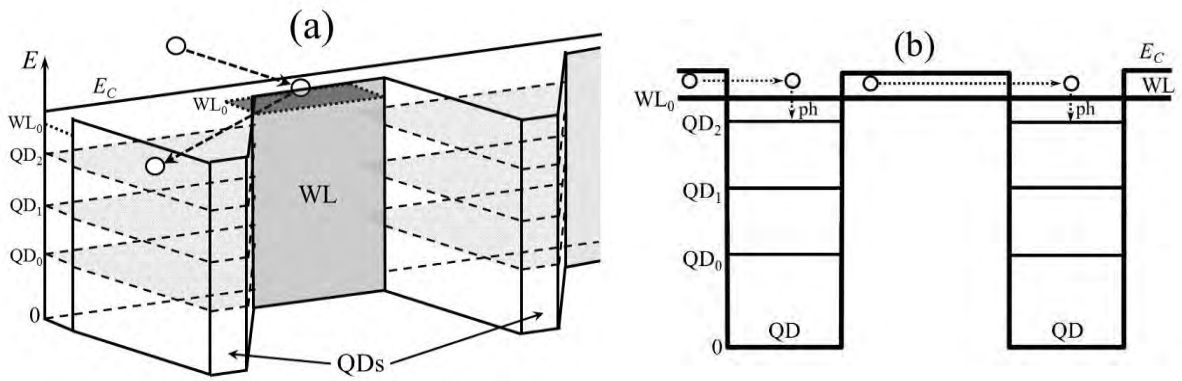

Figure 18. Capture of a photoelectron into QD via WL (a); electron levels in QDs and WL (b).

In **Fig. 19**, the PL spectrum of the medium with QDs between $Al_{0.2}Ga_{0.8}As$ bottom and top nanometer layers shows the absence of the peak at 930 nm, which is observed in QD media grown without $Al_{0.2}Ga_{0.8}As$ layers. It is also seen that QD ground-to-ground peak is significantly red-shifted compared to other QD media. This evidences that QDs formed on GaAs surface have larger size.

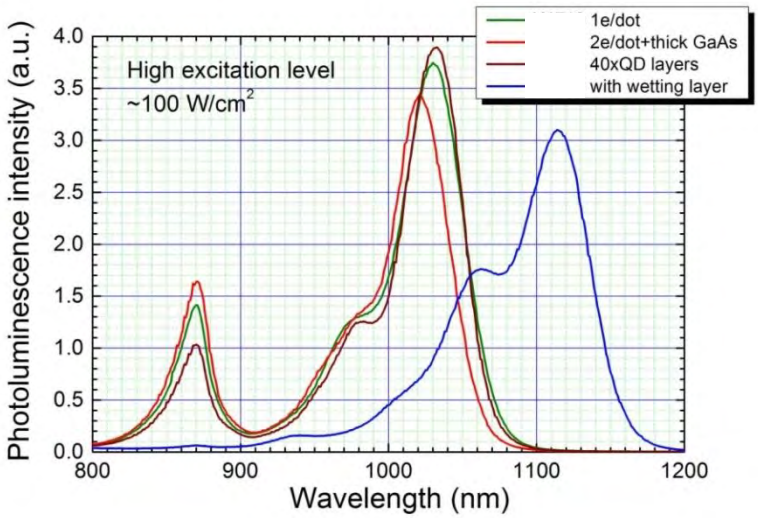

Figure 19. Photoluminescence of QD media with WL (blue) and without WL (green, red, brown).

4.3. Enhancement of IR Photoresponse due to Nanoscale Potential Barriers

To investigate effects of the built-in-dot charge on the unipolar kinetics in QD photodetectors, we investigate anisotropic potential barriers in real QD structures used for IR sensing

Our QD structures have been fabricated using molecular beam epitaxy with growth temperatures of 500 ± 10°C, as it was discussed in **Section 3.3**. InAs dots were grown on AlGaAs surfaces by deposition of approximately 2.1 monolayers of InAs. The obtained structures were doped in two

different ways: with intra-dot doping (devices B44 and B52) and with inter-dot doping (devices B45 and B53). In devices B44 and B52 (**Fig. 20a**) the dopant sheet concentration was 2.7×10^{11} cm^{-2} and 5.4×10^{11} cm^{-2}, respectively. Devices B45 and B53 have been grown with Si dopants directly in the middle of each AlGaAs barrier layer (**Fig. 20b**).

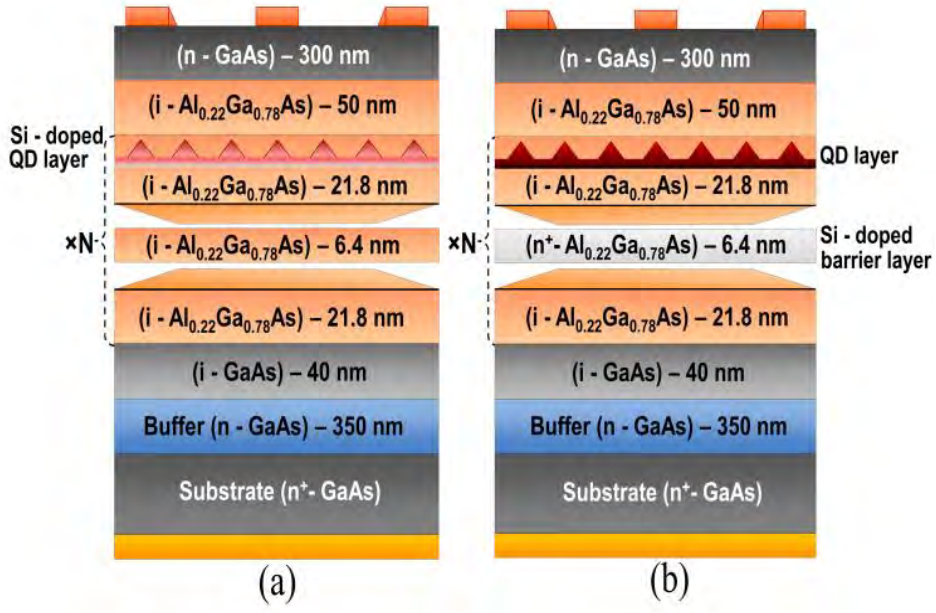

Figure 20. Quantum-dot structures with intra-dot doping, i.e. doping of QD layers (a) and inter-dot doping, i.e. doping between QD layers (b).

In devices B45 and B53 the dopant sheet concentration was 2.7×10^{11} cm^{-2} and 5.4×10^{11} cm^{-2}, respectively. QDs had truncated pyramid shape with average 3.6 nm height and 15 nm width. The QDs were distributed over QD layer randomly. The average distance between dots was 31 nm which corresponds to the sheet concentration of $10^{11}cm^{-2}$. Parameters of our samples are summarized in Table 1.

Table 1. QDIP devices.

Device	**B44**	**B45**	**B52**	**B53**
Doping	**intra-dot**	**inter-dot**	**intra-dot**	**inter-dot**
Donor concentration (10^{11} cm^{-2})	**2.7**	**2.7**	**5.4**	**5.4**
Number of electrons in dot, *n*	**2.7**	**2.8**	**4.7**	**6.1**
Built-in-dot charge, n_q	**1.8**	**2.8**	**3.45**	**6.1**

To calculate the built-in-dot charge and investigate the potential profiles around dots, we used the nextnano[3] software, which allows for simulation of multilayer structures combined of different materials with realistic geometries in one, two, and three spatial dimensions (see **Section 3.2**). We simulated the band structure and potential distribution in real devices taking into account the effects of contacts. As we discussed in Sec. 3.2, the potential barriers around QDs are strongly asymmetric. The barriers in the QD planes, i.e. in the direction perpendicular to the current, are substantially smaller than the barriers in the direction of the current. This asymmetry has strong consequences for the kinetics of photoelectrons. In **Fig. 21**, we compare the potential profiles in the A-B cross-section (x-axis) and in the C-D cross-section (z-axis) that are shown in **Fig. 8**. Potential barriers in the A-B cross-section are significantly smaller and, therefore, they are presented with higher resolution.

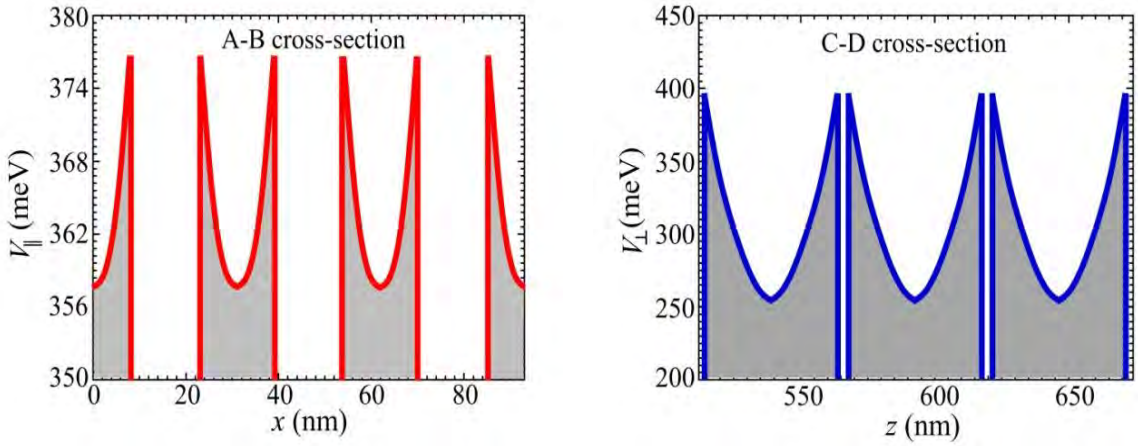

Figure 21. Potential barriers around dots at the center of QD structure in the A-B cross-section (x-axis) and in the C-D cross-section (z-axis).

Using the nextnano[3], we have analyzed the local potential barriers around single quantum dots as a function of the built-in charge. As it is expected, these local barriers are independent on the QD position in the device and strongly asymmetric, because of the asymmetry of QD shape.

Figure 22 shows the height of local potential barriers around single dots in the directions perpendicular and parallel to QD planes as a function of the built-in-dot charge. Linear character of dependences is expected. In **Fig. 22**, we highlight the strong anisotropy of the barriers, which is critically important for capture processes and photoelectron kinetics.

As it is shown in **Fig. 22**, the height of the potential barrier in the direction parallel to the QD plane is substantially smaller than that in the perpendicular direction. Therefore, we expect that the capture processes in QD planes will dominate in the relaxation processes. According to **Fig. 20**, the corresponding barrier height is proportional to the built in dot charge, n_q, with the proportionality coefficient $b = 2.5$ meV. In the case of the intra-dot doping, the dot charge n_q is equal to the dot population, n, reduced by the number of dopants, p, in the dot, i.e. to $n_q = n - p$. In the case of the inter-dot doping, the built-in-dot charge q is obviously equal to n.

Thus, according to Eq. 4 we expect that the effects of doping on the photocurrent in QD structures are described by:

$$I = A\, n \exp\left(\frac{b n_q}{k_B T}\right). \qquad (5)$$

Here, A is some constant which does not depend on doping. The pre-exponential factor in Eq. (5) describes the increase of the absorption with increasing number of electrons in the dot, n. The exponential factor describes the effect of potential barriers around dots on the photoelectron lifetime. It is proportional to the dot charge, n_q, determined by the number of electrons and number of dopants in the dot.

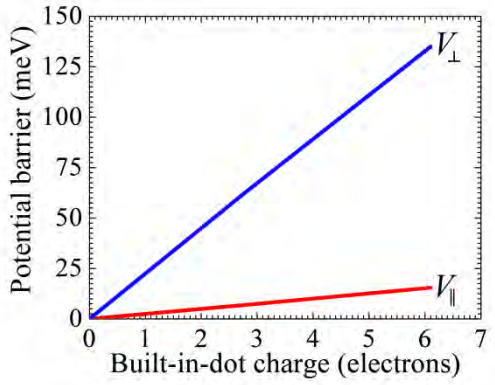

Figure 22. Height of potential barriers around singles dots in the directions perpendicular and parallel to QD planes.

In **Fig. 23**, we apply the analysis of our experimental data in the framework of this model. For fitting of our experimental results, we use n and n_q, calculated with nextnano[3] (see Table 1). As seen, the theoretical modeling (*red circles*) is in a very good agreement with experimental data (*blue squares*). From this fitting, the parameter b was found to be equal to 2.7 meV, which is in a good agreement with b = 2.5 meV that we obtained from the independent modeling of the potential barrier heights (see **Fig. 22**).

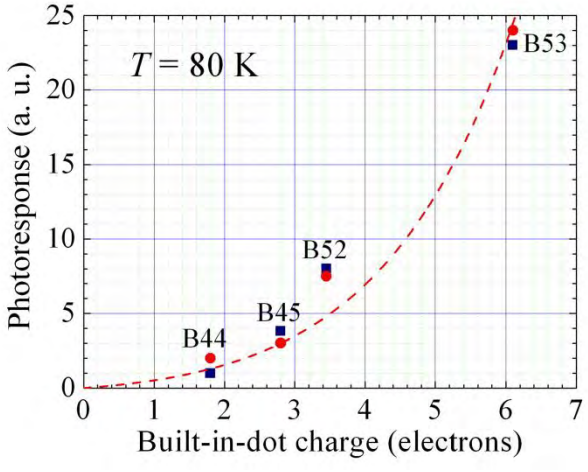

Figure 23. The photocurrent as a function of the built-in-dot charge. The blue squares are for experimental data and the red circles are for modeling results. The red dashed line is the theoretical dependence for the inter-dot doping.

The *red dashed line* shows the modeling results for the inter-dot doping ($n = n_q$), which was used for doping samples B45 and B53. For samples B44 and B52 with the doping of QD layers, the dot charge was formed by the electrons captured in the dot and dopants placed in the dot. In this case, $n = n_q + p$ and the corresponding *red circles* are above the dashed line.

Thus, the proposed, relatively simple model provides very good description of doping effects on the photoresponse of QD structures. Such good agreement with experiment evidences that the model adequately takes into account the main effects of doping on photoelectron kinetics.

Thus nanoscale barriers provide strong improvement in responsivity of quantum-dot infrared photodetectors. We demonstrate ~25 times increase of the photoresponse of QDIP, when the built-in-dot charge increases from 1 electron to 6 electrons per dot.

4.4. Electric Control of IR Properties of Nanomaterials

Quantum well IR photodetectors (QWIP) have attracted considerable attention due to a variety of applications such as remote sensing, thermal imaging, industrial and environmental monitoring. The well-established growth and processing techniques of the A_3B_5-based heterostructures (see **Sec. 3.3**) open a wide range of possibilities for bandgap engineering and intersubband transitions for detection of IR radiation. QWIPs are promising candidates for multi-color sensing in the spectral range from THz to mid-IR. Voltage-switchable and voltage-tunable QWIPs have been studied in a number of works. Various approaches for the design of voltage-tunable and voltage-switchable QWIPs have been proposed. Following to our main idea we combine the bandgap engineering with engineering of tunable nanoscale profile. In the project research we have demonstrated that more effective voltage tunability and switching are realized in asymmetrically doped Double Quantum Wells (DQWs) due to superposition of external field with doping-induced built-in electric field. Asymmetrical doping of DQW structure provides two-color sensing as well as voltage switchable and voltage-tunable photoresponse.

The DQW were formed by 25 identical stages. The potential profiles of left-most and right-most DQWs are slightly different due to contacts. The DQWs have been designed to support solely two intersubband transitions from ground states to the excited states. Therefore, the photoresponse to IR radiation has two spectral components. Both components are strongly affected by the bias voltage V_b.

The schematic epitaxial layer structure of a device with high tunability is shown in **Fig. 24**. It is based on the coupled quantum wells composed of a 6.5 nm GaAs layer Si-δ-doped with sheet concentration 5 10^{11} cm^{-2} and a 6.5 nm undoped GaAs layer separated by a 3.1-nm-thick $Al_{02}Ga_{08}As$ layer. The device consists of 25 DQW stages separated by 50 nm $Al_{02}Ga_{08}As$ barriers.

To provide effective coupling of IR radiation to our QWIP devices, we compare the following two schemes. In the first scheme, the radiation is incident on the 45°-angle facet of substrate and in the second scheme the coupling to normal incident radiation is enhanced by the diffuse reflector (**Fig. 25**). Without diffuse reflector, the coupling to normally incident IR radiation, associated with a violation of the polarization selection rule for inter-subband transitions, is small.

To calculate the photo-induced transitions we performed self-consistent calculations, which take into account charge redistribution in asymmetrically doped DQWs. For our calculations we used the nextnano3 software (see Sec. 3.2.) which is a flexible and effective tool for the analysis of

photodetectors. Our modeling shows that tunability is improved in structures where the excited states are located close to the extended states.

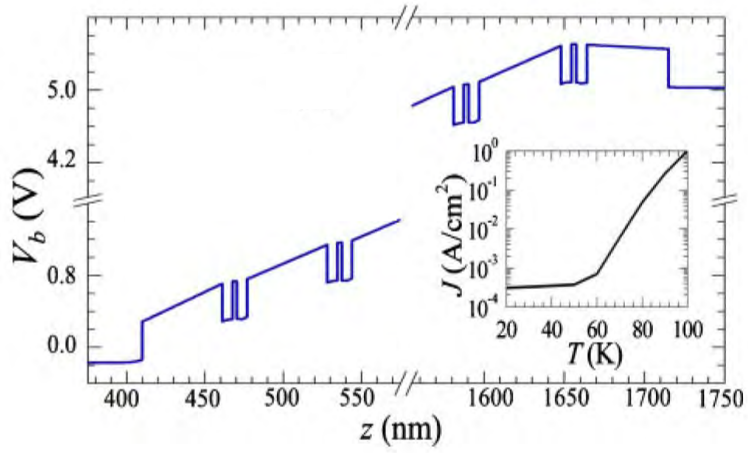

Figure 24. Energy band diagram of 25 period DQW structure under bias V_b = +5 V. Inset shows dark current density, J, versus temperature, T, at bias V_b = +3 V.

Figure 26 presents the conduction band diagram of a single stage, which consists of two coupled QWs. In this figure we also demonstrate modification of wave functions and the energy levels due to the bias voltage (V_b = -5, 0, and +5 V). The calculated populations of the first two tunnel-coupled levels at T = 70K as a function of the voltage are as follows: 99 and 1%, 95 and 5%, and 76 and 24%, at -5, 0, and +5 V, respectively. One can see that there is almost no redistribution of electrons between levels for negative V_b, while for positive V_b a significant redistribution of electrons takes place when tunnel coupling increases. Strong coupling of levels near the top of quantum wells is realized for even at small V_b since these states are connected to the continuum. Since only the right quantum well is doped, the DQW's band diagram is asymmetric at V_b = 0 due to the built-in electric field contribution.

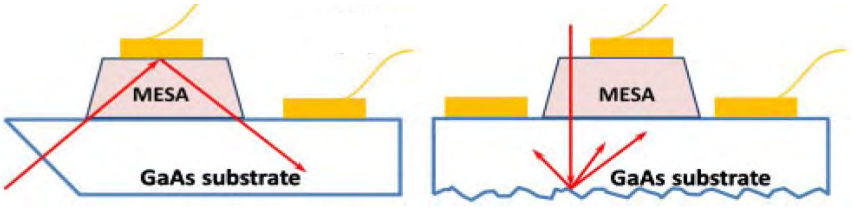

Figure 25. Schematic view of photoexcitation geometry through substrate with 45°-angle facet (left) and under diffuse reflection of normally incident radiation (right).

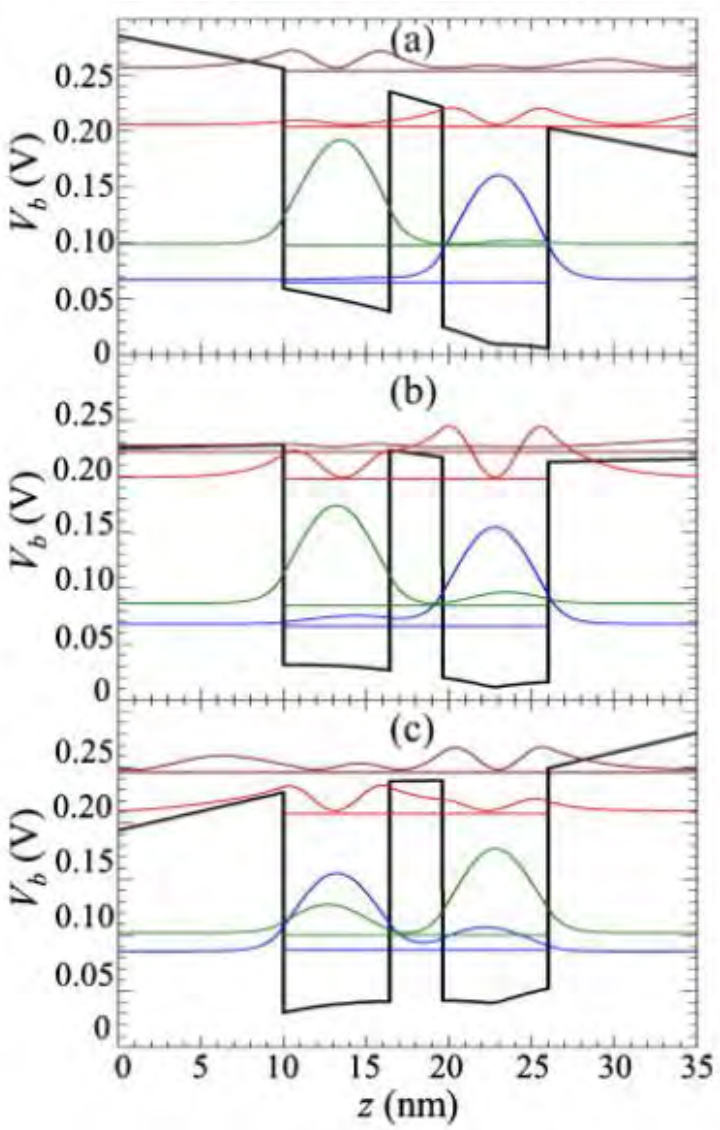

Figure 26. Self-consistently calculated potentials and wave functions of the ground and excited states in DQWs at T= 70K under V_b = -5 (a), 0 (b), and +5V (c). The relative populations of the first two tunnel-coupled levels are: 99 and 1% (a), 95 and 5% (b), and 76 and 24% (c), respectively.

The modeling shows larger peak-shift under negative bias which is more symmetric since the built-in electric field compensates the applied bias. In principle, there are four possible transitions between two deep and two shallow levels in a single detection unit. A two-color photoresponse is found because only the lowest level is populated under negative bias [see **Fig. 26a**]. Under positive bias the transitions from the lowest excited state to the extended states via tunneling processes are suppressed and thermoexcitation processes are limited by relatively high barrier [**Fig. 26c**].Therefore, the lowest excited state weakly contributes to the photocurrent. Using this mechanism the two-color operation is realized in asymmetrically doped DQW structure.

To characterize IR nanomaterial with asymmetrically doped DQWs, we measured dark current-voltage characteristics, responsivity, and spectral characteristics of photoresponse. The device was mounted inside the cryostat with a KBr window which has 90% transmissivity in the mid-IR range. A Ge filter was placed between the cryostat and globar to rule out the absorption by the interband transitions. The sample temperature was measured and controlled by Cryocon temperature controller. The current-voltage curves were registered by the Keithley 2602 source-meter with accuracy of 10^{-7} A/cm^2. The schematic of the measurement setup is shown in **Fig. 27.**

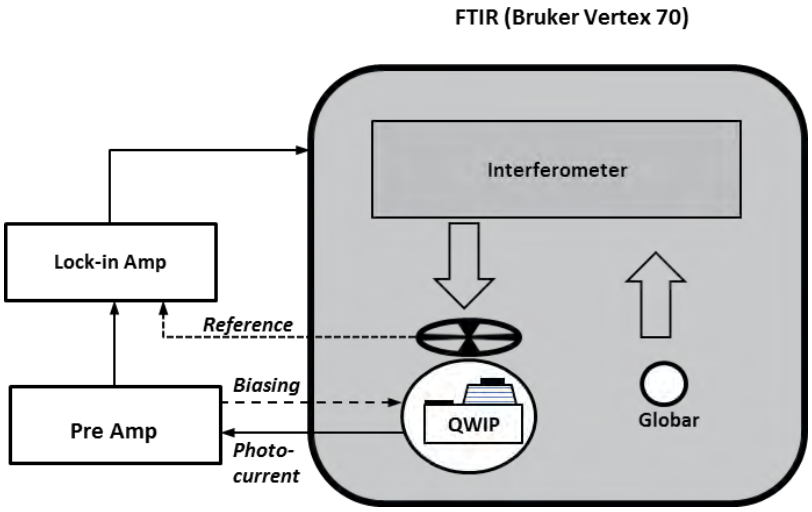

Figure 27. The setup for the IR photoresponse measurements.

The measured dark current and noise current as a function of the bias voltage are presented in **Fig. 28.** The dark current as a function of bias voltage was measured from 78 to 140 K. As seen, the dark current under positive bias is slightly higher than that that under negative bias. Usually this asymmetry is stronger and associated with the dopant migration in the growth direction. We believe that in our structures the effect of dopant migration is substantially compensated by the asymmetric doping.

The voltage tunability of the photoresponse spectrum is mainly defined by three mechanisms. First, the electron energy levels are shifted due to the Stark effect. Second, the applied electric field causes a charge redistribution in the coupled wells and shift of electron energy levels due to modification of selfconsistent potential. Third, the electric field enhances tunneling and thermo-activation processes due to a reduction of the width and height of the triangular barriers which separate extended states from excited states. We limited our research by relatively low fields that do not generate electric field domains and other instabilities.

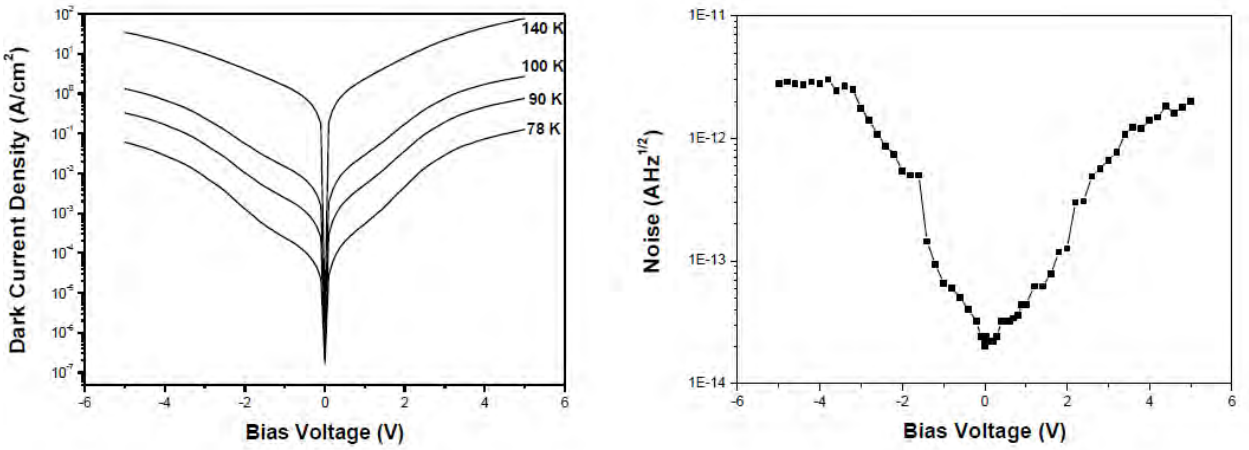

Figure 28. The dark current vs bias voltage at 78, 90, 100, and 100 K (a), and the noise current at 78 K vs bias voltage (b).

The spectral changes of the photocurrent were reliably measured for both bias polarities. As it is shown in **Fig. 29**, the spectral characteristics of the photoresponse strongly depend on the polarity of the bias voltage due to asymmetric doping. Below 70K we observe two distinctive peaks. At negative bias these two peaks are centered near 7.9 and 10.3 μm wavelengths. These peaks can be attributed to the transitions from the lowest ground state to the excited states that are effectively coupled to the extended states. Evolution of spectral characteristics with increase of the negative bias voltage is presented in **Fig. 30**.

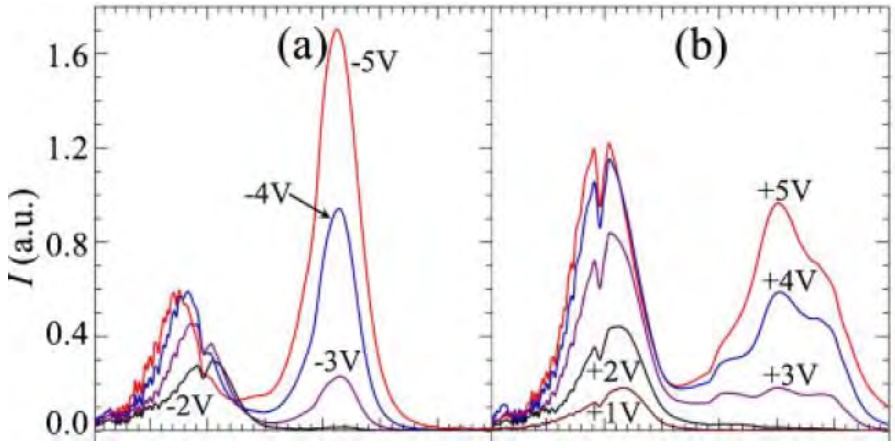

Figure 29. Spectral dependencies of photocurrent under negative (a) and positive (b) bias voltages for the cases of photoexcitation under diffuse reflection of normally incident radiation.

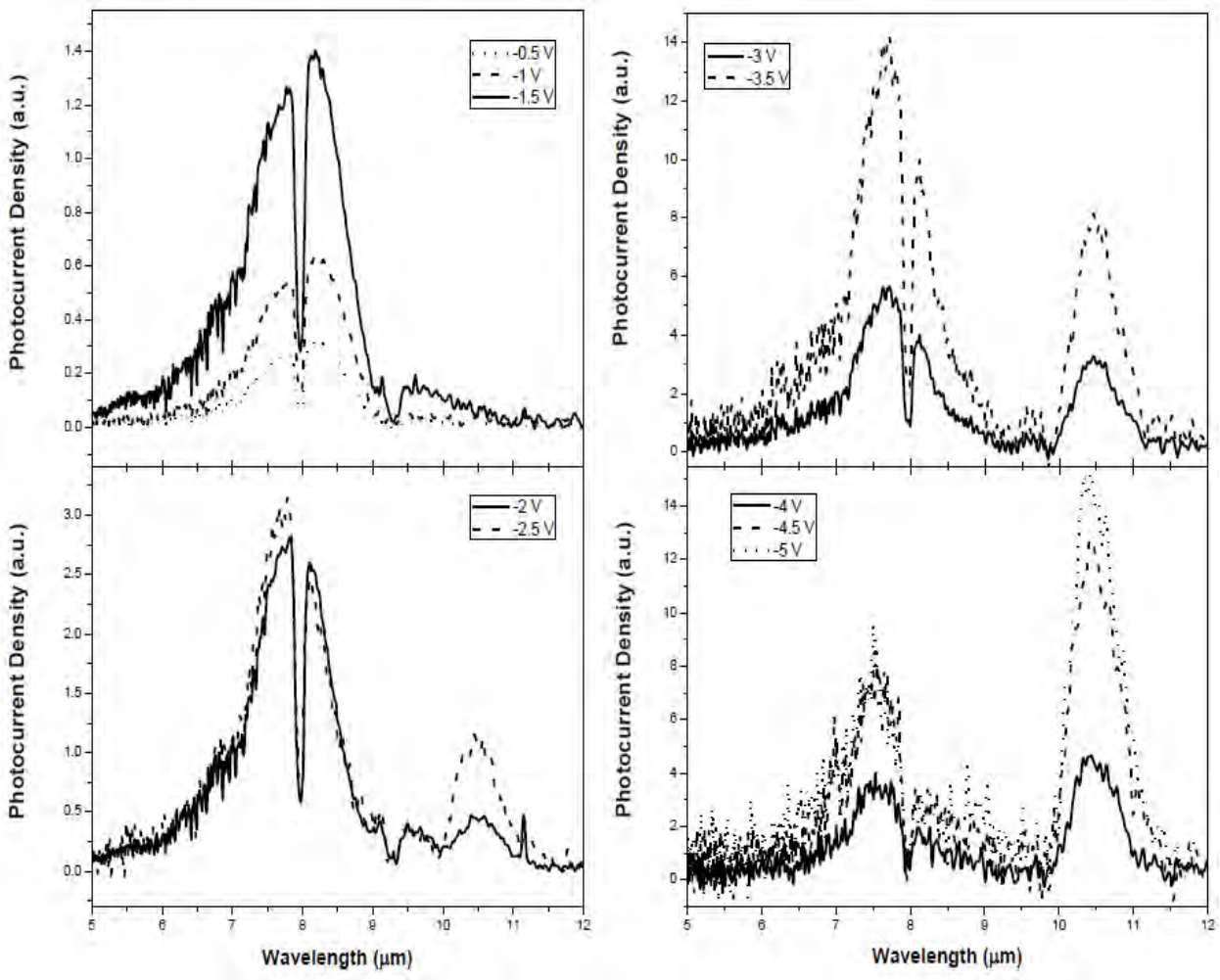

Figure 30. Spectral dependencies of the photoresponse at negative bias voltages of 0.5, 1, 1.5, 2, 2.5, 3, 3.5, 4, 4.5, and 5 V

For an intermediate bias (V_b = - 3 V) both spectral peaks are observed with small overlap. The intensities and widths of the peaks depend on bias voltage. The peak around 10.3 μm, observed only at large magnitude of bias voltages [V_b < -2.6 V], is caused by the suppression of the tunneling processes. At low bias voltages [see the band diagram in **Fig. 24**], the photocurrent is blocked by the 50 nm $Al_{02}Ga_{08}As$ barriers. However, when increasing the positive bias, the tunneling barrier is lowered down and carriers can escape the quantum wells increasing the photocurrent. The main spectral peaks (7.5 and 10.3 μm under negative bias) shift to 8.3 and 11.1 μm under positive bias. For the same reason as the peak at 10.3 μm is only visible at high negative bias voltage, the photocurrent peak around 11 μm appears only at a large magnitude of the applied positive bias (V_b > 3 V). Since the upper levels transform into extended states for positive bias, the width of peak increases.

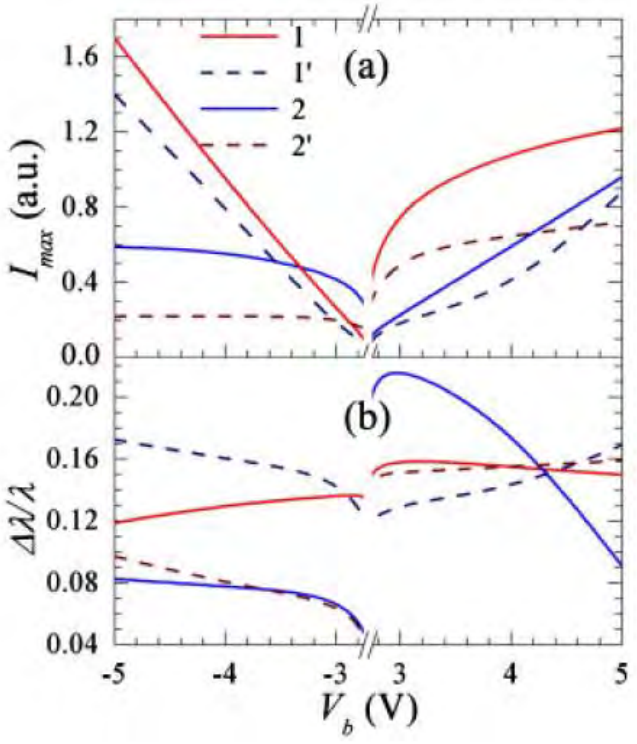

Figure 31. (a) Amplitudes of low- and high-energy peaks of photocurrent (marked as 1 and 2, respectively) versus V_b. (b) Widths of these peaks versus V_b. Solid (1 and 2) and dashed (1' and 2') curves correspond to the cases of photoexcitation under diffuse reflection of normally incident radiation or through 45°-angle facet, respectively.

The amplitudes of high- and low-energy peaks of photocurrent differ up to 2 times under negative bias and about 30% under positive bias [**Fig. 30a**]. The bias voltage dependences are different for $V_b > 0$ and $V_b < 0$ because of the doping asymmetry. For the same reason, the widths of peaks are also different. For the same reason, the widths of peaks are also different, as it is shown in **Fig. 30b** where the relative widths $\Delta\lambda/\lambda$ are plotted versus V_b. For negative bias the high-energy peaks sho narrower linewidth $\Delta\lambda/\lambda = 0.07 - 0.1$ due to transitions between localized states. The linewidths $\Delta\lambda/\lambda$ are about 0.15 for the low-energy peak and for both peaks at positive bias. In addition, $\Delta\lambda/\lambda$ increases up to 0.2 at V_b above 3V, when the photoresponse is suppressed.

Spectral and bias dependences of photocurrent are summarized by the contour plots shown in **Figs. 32a** and **32b** for the both cases of photoexcitation. The largest peak shifts occur at $V_b < 0$ because the doping-induced internal electric field is added to bias voltage and the quantum confined Stark effect is more pronounced. Also the short wavelength peaks have larger peak-shift than the long-wavelength ones because the transitions into extended states are more sensitive to applied voltage V_b. The behavior of photocurrent versus V_b and λ is similar to the corresponding transition energies calculated with our self-consistent simulation. In **Fig. 32** we plot both the transitions between localized states (solid curves) and transitions to extended states (dashed curves). Note, that these curves give the absorption peak positions while the photocurrent peaks are determined not only by absorption processes but also by thermal generation and capture processes. For this reason there is some difference between the calculated transitions and the photocurrent.

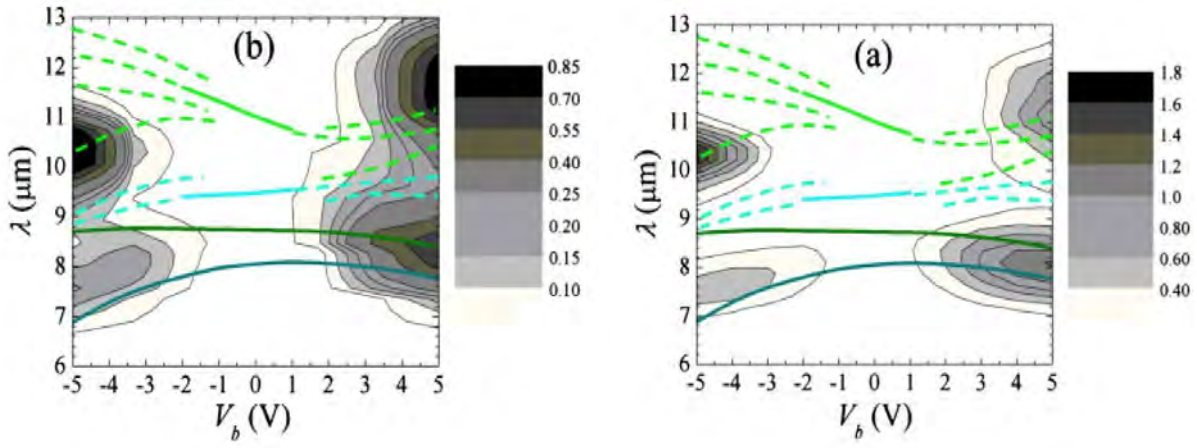

Figure 32. Contour plot of photocurrent versus V_b and wavelength, λ, for the cases of photoexcitation under diffuse reflection of normally incident radiation (a) or through 45◦-angle facet (b). Solid and dashed curves correspond to transitions between localized states and from localized to extended states, respectively.

The presented above research results include designed, grown, and characterized a two-color QWIP based on intersubband transitions in asymmetrically doped coupled QWs. In these structures the effects of electric field on electron states (Stark effect), tunneling processes (Fowler–Nordheim effect), and thermoactivation processes (Poole–Frenkel effect) are enhanced by the asymmetrical doping. These effects provide an effective voltage tunability of spectral photoresponse. In our devices the spectral peaks switch from ~7.5 to ~ 11.1μm by reversing the bias polarity. The spectral characteristics are controlled at the intermediate bias voltages. Further improvements in tunability are expected at higher doping levels. In future, these relatively simple and highly scalable devices may be used in multi-element imaging arrays for multi-spectral sensing.

4.5. Optical control of IR nanomaterials

As we discussed in previous sections, the n-charging of QDs strongly enhances the IR absorption. Optical bias creates electron-hole pairs localized in the dots and in this way provides effective and tunable control of IR absorption. The process of optically induced IR absorption in the n-charged QD is shown in **Fig. 33**.

As discussed above, to stimulate electron transitions by IR radiation, additional electrons should be placed in QDs. Corresponding processes in n-doped QD structures are presented in **Fig. 33a**. Due to IR induced transition (the red arrow) the photoelectron is excited from the ground state in QD to a high energy state, which is separated from the conducting state by thin potential barrier. The barrier may be overcome via tunnelling process (the grey arrow) or via thermoemission. **Figure 33b** shows the optical control of the processes of IR absorption. First, the optical radiation creates an electron-hole pair, presumably in the ground state of the QD. Then, the electron is excited due to the resonance IR absorption. The optical bias of IR absorption may be considered as an optical doping.

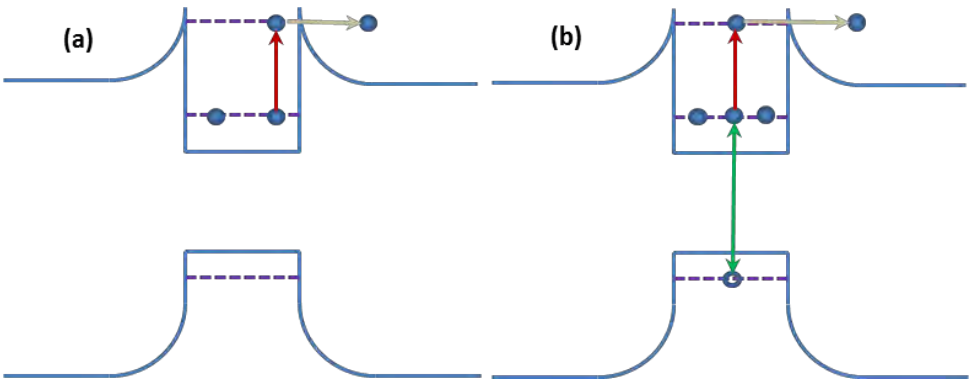

Figure 33. Optical control of IR photodetectors: (a) IR absorption and tunnelling in n-doped QD, (b) optical bias of IR absorption.

We investigated the effect of the optical bias in the InAs/AlGaAs QD structures with modulation-doped with Si in the middle of the AlGaAs barrier layers (a doping sheet concentration of 2.7×10^{11} cm^{-2}). A red LED with 620 nm wavelength was used for optical bias.

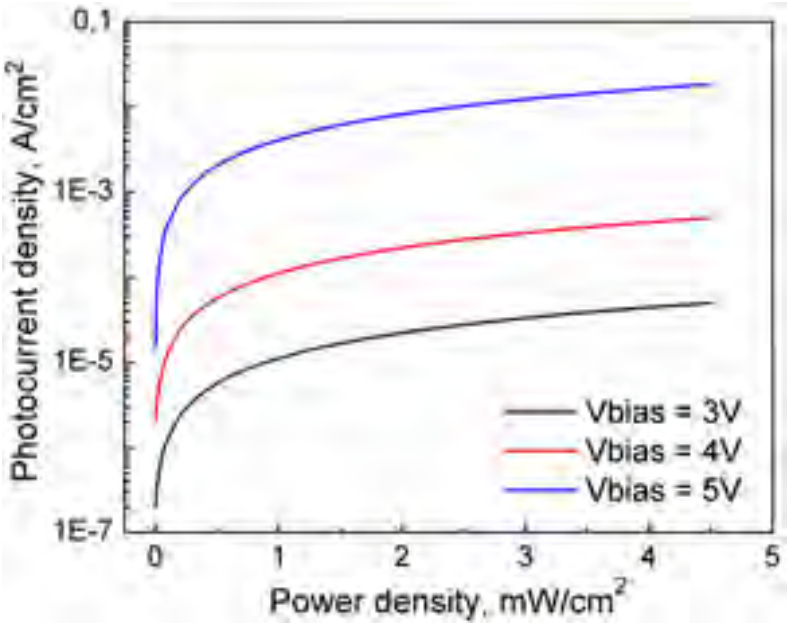

Figure 34. Photoresponse to the 4.3micron IR radiation at 77K of the QD structure as a function of optical bias.

Fig. 34 shows the photocurrent induced by 4.3 micron IR radiation that corresponds to inter-subband transitions in the QDs. In this experiment, the IR signal was modulated and corresponding photocurrent was measured with lock-in amplifier. The measurements at 77 K demonstrate the increase of photocurrent by orders of magnitude due to the optical bias. This

observation manifests the strong enhancement of the IR electron transitions from the localized states in QDs to the conducting states in the matrix.

4.6 Perspectives of 2DEG Materials for IR Sensing

4.6.1 Infrared Detectors based on p-i-n Multiple-Graphene-Layer Nanostructures

Development of advanced IR sensing technologies is critically important for a number of applications, including environmental and industrial monitoring, homeland security, biosensing, imaging, and communications. For these applications two-dimensional materials can offer substantial advantages compared with traditional 3D materials. First of all, the small electron densities per square lead to small electron noise and increase the detector sensitivity. Plasmons in these structures may be used for enhancement of resonant absorption, which spectral characteristics are tunable by a gate. High functionality of 2D materials and variety of photoresponse mechanisms allows for design fast detectors with moderate sensitivity as well as slow high sensitive detectors. Single graphene layers may be used for a variety of photonic components, which create advanced technological platform for advanced detection.

The use of the multiple graphene layer (MGL) structures opens up prospects of further enhancement of capabilities of graphene-based optoelectronic devices, in particular, IR photodiodes. The graphene nano-ribbon (GNR) structures also exihibit the properties which are very useful for IR detection. The restoration of the energy gap in the GNR arrays, which is due to patterning of GL into GNRs, i.e., the formation of an array of quantum wires with the one−dimentional energy subbands, affects the density of states in the conduction and valence bands and, hence, the absorption spectrum and the photodetector spectral characteristics. The emerging of the energy gap promotes a substantial weakening of the inter-band tunnelling and, consequently, lowering of the dark current and enhancement of the detector detectivity. By virtue of the energy gap in GNR structures, they can be used not only for photodiodes but also for phototransistors.

We have proposed and investigated the novel concepts of FIR photodetectors utilizing MGL and GNR structures: the MGL p-i-n photodiode and the GNR p-i-n photodiode. We have developed the device models for MGL and GNR photodiodes and compare their characteristics. We have found that the MGL and GNR photodiodes can surpass state-of-the-art photodetectors in responsivity and detectivity, especially, at elevated temperatures.

Figure 35 shows the structures of MGL and GNR p-i-n photodiodes. In these devices, the MGL and GNR structures are supplied by the side ohmic contacts (source and drain) between which the bias voltage V is applied [see **Fig. 35a].** The number (K) of GLs in the MGL photodiodes can vary from one to dozens. The formation of the p- and n-regions in both MGL and GNR photodiodes can be associated either with the chemical doping as shown in **Figs.35a** and **35c** or using the special gates (separated by the gate layer), to which the dc voltages are applied as shown in **Figs. 35b** and **35d**. In the latter case, the side sections of GLs and GNRs are occupied by electrons and holes induced by the transverse electric fields associated with the applied gate voltages. The potential profiles in the device with electrically induced p-i-n junctions in GLs, which are located at different depths from the MGL structure top, are shown in **Fig. 36b.** The heights of the barriers μ_k (where k =1, ..., K is the GL index) at the p-i and i-n junctions are different because the screening of the transverse electric field results in different electron and hole densities and their Fermi energies beneath the gates. In the MGL photodiodes with the chemically doped p- and n-regions, these regions can create the barriers with equal height. As it

can be seen in **Fig. 36c,** the bias source−drain voltage drops primarily across the i−region (only the potential profile in the top−most GL is shown). This leads to the built-in electric field in the i-region.

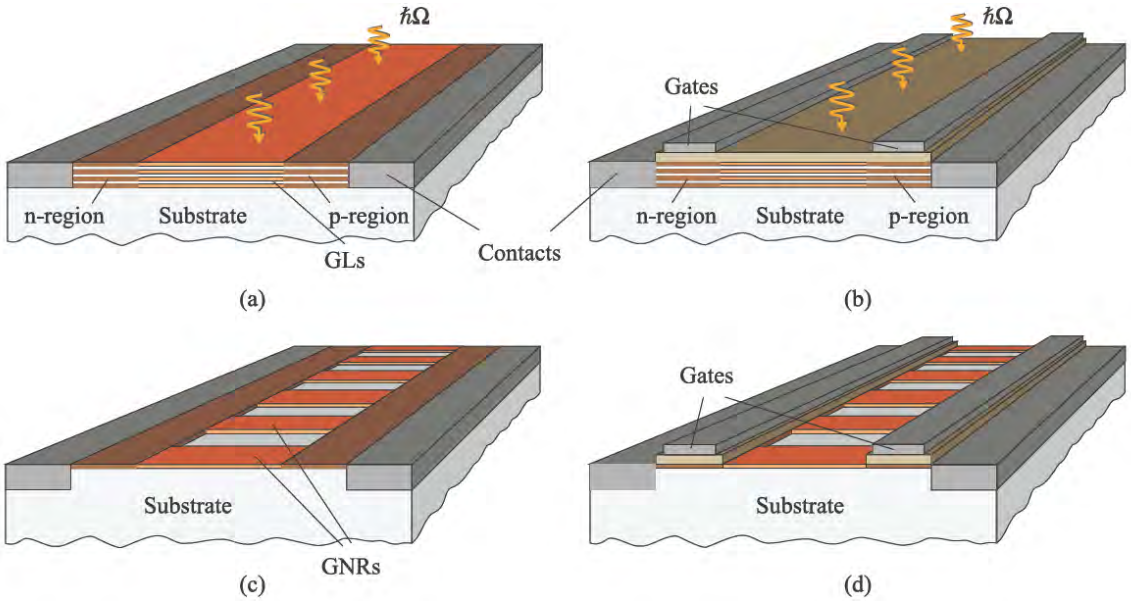

Figure 35. Schematic views of MGL p-i-n photodiodes with (a) chemically doped p- and n-regions and (b) electrically induced p- and n-regions (electrical doping), as well as of GNR p-i-n photodiodes with (c) chemically doped p- and n-regions and (c) electrically induced p-and n-regions, respectively.

As it is shown in **Fig. 36**, the operation of the MGL p-i-n photodiodes is analogous to that of the traditional p-i-n photodiodes. The electrons and holes generated by the incident radiation are driven to the n− and p−regions, respectively, by the built-in electric field. The motion of the photo-generated electron and hole creates the signal current induced in the external circuit. Due to the gapless energy spectrum of MGLs, the photo-generation in the i-region occurs even at rather low energies of incident photons.

We have calculated the responsivity and detectivity of MGL photodiodes (see example in **Fig. 37**). Below we compare their characteristics with the mercury-cadmium−tellurium (MCT) photodiodes. Both of them can exhibit similar quantum efficiencies. However, the dark current associated with the thermo-generation of electrons and holes, i.e., the factor crucially affecting the detectivity, in GNR photodiodes, should be much lower than in MCT photodiodes. This is because the energy of optical phonons in MGLs is much larger than optical phonon energy in MCT. As a result, even at the room temperatures, the number of optical phonons in MGL photodiodes is small. Therefore, the thermo-generation associated with the absorption of optical phonons in GLs is relatively weak. Next mechanism which could contribute to the thermo-generation in GLs is the absorption of acoustic phonons. However, due to small velocity of acoustic waves in comparison with the characteristic velocity of electrons and holes in GLs, the one-phonon interband absorption is forbidden. The Auger processes, which are fairly strong in MCT, are also forbidden in GLs due to the linear dispersion relation for electrons and holes.

Thus, one can expect that MGL and GNR photodiodes can substantially surpass MCT photodiodes in the dark-current limited detectivity.

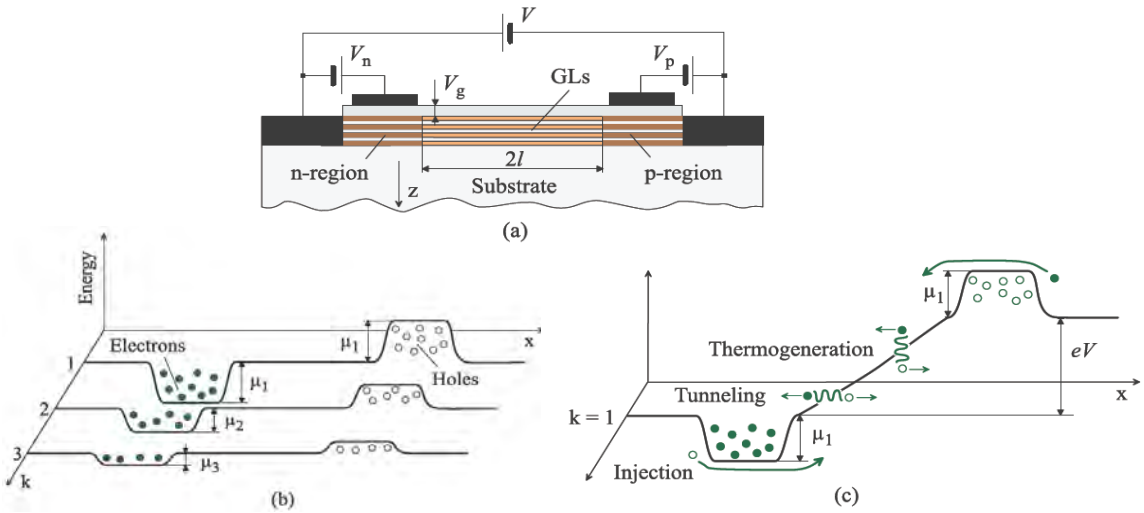

Figure 36. (a) Structure of MGL photodiode with electrically induced p-and n-regions and the pertinent wiring, (b) energy band diagrams of GLs located at different distances from the top at $V = 0$, and (c) energy band diagram of the top−most GL at reverse bias. Opaque and open circles correspond to electrons and holes accumulated beneath the positively and negatively biased gates, respectively. Arrows show their intraband and interband transitions at dark conditions.

As it is shown in **Fig. 36**, the operation of the MGL p-i-n photodiodes is analogous to that of the traditional p-i-n photodiodes. The electrons and holes generated by the incident radiation are driven to the n− and p−regions, respectively, by the built-in electric field. The motion of the photo-generated electron and hole creates the signal current induced in the external circuit. Due to the gapless energy spectrum of MGLs, the photo-generation in the i-region occurs even at rather low energies of incident photons.

We have calculated the responsivity and detectivity of MGL photodiodes (see example in **Fig. 37**). Below we compare their characteristics with the mercury-cadmium−tellurium (MCT) photodiodes. Both of them can exhibit similar quantum efficiencies. However, the dark current associated with the thermo-generation of electrons and holes, i.e., the factor crucially affecting the detectivity, in GNR photodiodes, should be much lower than in MCT photodiodes. This is because the energy of optical phonons in MGLs is much larger than optical phonon energy in MCT. As a result, even at the room temperatures, the number of optical phonons in MGL photodiodes is small. Therefore, the thermo-generation associated with the absorption of optical phonons in GLs is relatively weak. Next mechanism which could contribute to the thermo-generation in GLs is the absorption of acoustic phonons. However, due to small velocity of acoustic waves in comparison with the characteristic velocity of electrons and holes in GLs, the one-phonon interband absorption is forbidden. The Auger processes, which are fairly strong in MCT, are also forbidden in GLs due to the linear dispersion relation for electrons and holes.

Thus, one can expect that MGL and GNR photodiodes can substantially surpass MCT photodiodes in the dark-current limited detectivity.

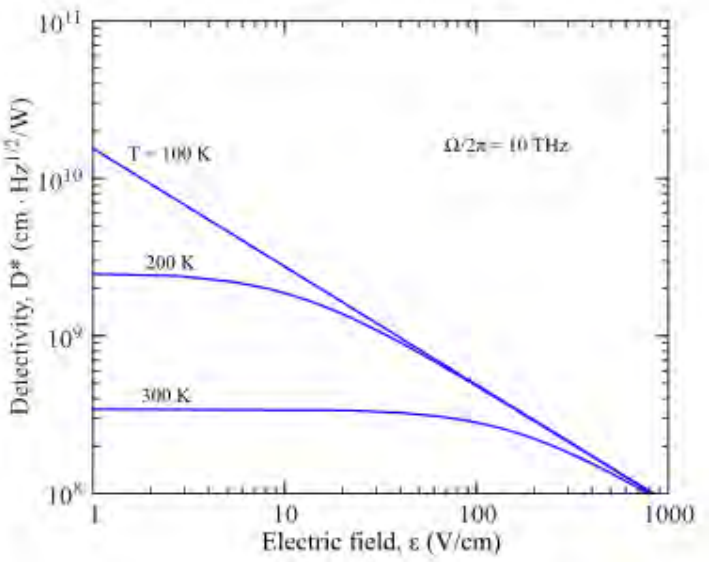

Figure 37. MGL photodiode detectivity as a function of the electric field at different temperatures.

Comparing MGL IR detectors with QWIPs and QDIPs, we should highlight that the absorption coefficients in QW and a QD arrays is about one order of magnitude smaller than in a GL. The thermo-excitation rate in QWIPs and QDIPs due to the absorption of optical phonons appears to be much higher than in MGL and GNR photodiodes. Also, the tunneling from QWs and QDs can also greatly contribute to the dark current limiting the QWIP/QDIP performance.

Summarizing this section, let us highlight that due to high values of the quantum efficiency MGL and GNR photodiodes can exhibit fairly high responsivity in the THz and IR ranges. It was shown that at room temperatures the thermo-generation of electrons and holes associated with optical phonon absorption is the dominant mechanism limiting the detectivity. However, taking into account relatively low probability of the optical phonon absorption in GLs and GNRs associated with rather large phonon energy, we found that the room temperature detectivity can be fairly high. The interband tunneling can be an essential mechanism determining the dark current and, hence, the MGL photodiode detectivity at lowered temperatures (T~250 K). This mechanism limits the ultimate values of the detectivity and necessitates the optimization of the device structure and proper choice of the temperature and the bias voltage. In contrast, in GNR photodiodes with an open energy gap, the interband tunneling can be insignificant even at rather strong electric fields (high bias voltages) in the i-region in a wide temperature range. Thus, these detectors can exhibit high responsivity and detectivity at elevated temperatures, in particular, at room temperatures, in a wide radiation spectrum range and can substantially surpass other detectors. The combination of high responsivity and detectivity together with spectral and polarization dependences make these detectors very promising for application in different

wideband (MGL photodiodes) and multi-color (based on GNR photodiodes with different width of GNRs) IR systems.

4.6.2 Graphene uncooled bolometers

We have proposed and analyze uncooled bolometric detectors based on GL structures. We demonstrate that such bolometers can exhibit fairly high responsivity, effectively operating at room temperatures and surpassing THz bolometers based on the traditional semiconductor heterostructures. The main advantages of GL-based room temperature bolometers are associated with the following three factors:

(i) high Drude absorption;
(ii) the dominant mechanism establishing the interband and intraband equilibrium is the interaction with optical phonons;
(iii) long time of the electron and hole energy relaxation via optical phonons.

Figures 38a and **38b** show the proposed nGL-GNR-pGL bolometers. The bolometers consist of two gapless n-type and p-type GL absorbing regions connected by undoped array of GNRs with sufficiently large energy gap, which serves as the barrier region. The GLs can be doped chemically (as in **Fig. 378a**) or ”electrically” (using the conducting gates with the bias voltages, as shown in **Fig. 38b**). The gates which control the electron and hole densities can be made from GLs. The energy barrier in such GNRs ensures a relatively strong dependence of the current on the effective temperature of electrons and holes enhancing the bolometer responsivity. **Figure 38c** shows the resulting device band structure at sufficiently large bias voltages.

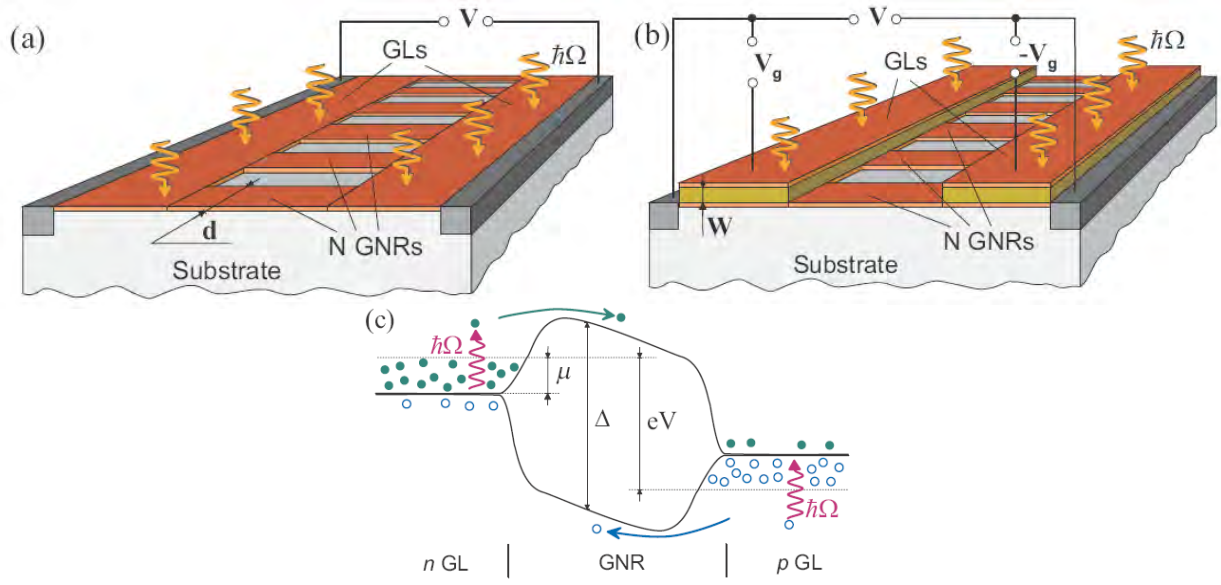

Figure 38. Schematic views of graphene bolometers with (a) chemically doped GLs, (b) electrically doped GLs,and (c) the bolometer energy diagram under bias voltage V (wavy arrows correspond to intraband transitions due to absorption of photons in GLs, smooth arrows indicate propagation of electrons and holes above the pertinent barriers in GNRs).

Due to relatively high electron and hole densities, the interelectron scattering time is sufficiently short to provide fast Maxwellization (or Fermization) of the photoexcited electrons and holes. Therefore, the electron and hole systems in GLs are characterized by quasi-Fermi energy μ and by the effective temperature T. The heating of the electron and hole gases in the pertinent sections, i.e., the deviation of the effective temperature T from the lattice temperature leads to the deviation of the Fermi energy μ from its equilibrium (dark) value μ_0.

Using the proposed device model, we calculate the dark current and the bolometer responsivity as functions of the GNR energy gap, applied voltage, and frequency. We have demonstrated that the proposed bolometer can surpass the bolometric detectors based on traditional semiconductor heterostructures.

4.6.3 Graphene vertical cascade IR photodetectors

We have proposed and evaluated the vertical intersubband IR photodetectors based on the Bernal-stacked multiple-GL structures with tunneling barrier layers using the cascade of the interband inter-GL radiative transitions The cascade of the electron tunneling and radiative-assisted tunneling processes supports the vertical dark current and photocurrent between the top and bottom GLs (playing the role of the emitter and collector). The advantages of these photodetectors include the voltage control of their spectral characteristics, a relatively high responsivity and detectivity (especially in the photodetectors with a relatively large number of GLs), a high speed of operation.

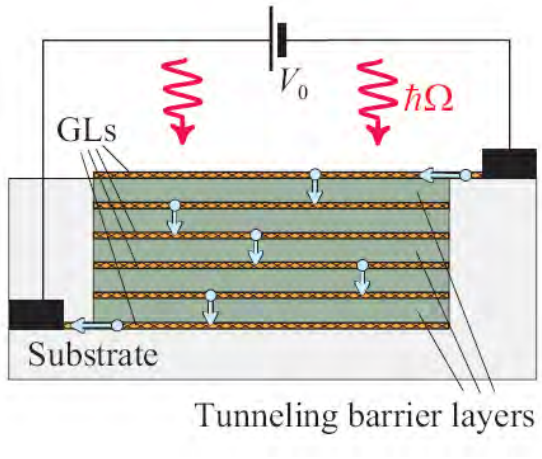

Figure 39. Schematic structure of a vertical I-GLPD with several (four) GLs.

Figure 39 shows the structure of the vertical intersub-band GL-photodetector (I-GLPD). It consists of several n-doped GLs separated by thin (tunneling-transparent) barrier layers of WS_2 or similar material. The bias voltage V_0 applied between the GLs serving as the emitter (top GL) and collector (bottom GL), respectively.

Figure 40 shows the device band diagram under bias (several GL-structure periods). As seen from **Fig. 40**, the energy gaps between the GLs are equal to $eV = eV_0/K$, where K = 1, 2, 3, ... is the number of the inter-GL barriers in the device. Absorption by the I-GLPD of the normally incident photons polarized in the GL plane. The absorption of a portion the photons is accompanied by the electron transitions between the neighboring GLs (see the wavy arrows in **Fig. 40**). Such direct but inter- GL transitions produce the inter-GL photocurrent.

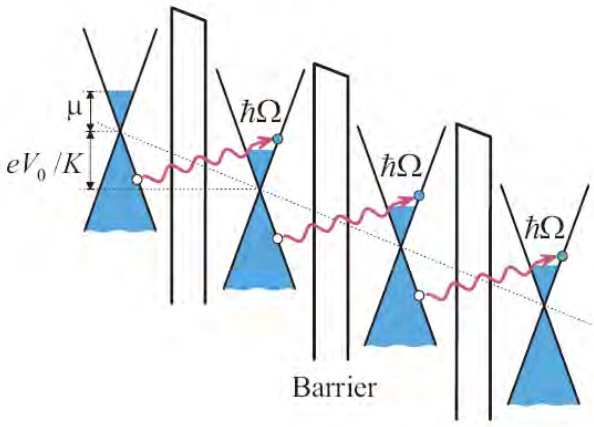

Figure 40. Band diagram of a I-GLPD under applied bias. The arrows indicate the radiative interband transitions from upper to lower GLs (which provide the main contribution to the photocurrent).

We calculated the responsivity and detectivity for the vertical cascade interband GL-photodetectors with different number of GLs and doping levels at different bias voltages in a wide temperature range (as example see **Fig. 41**).

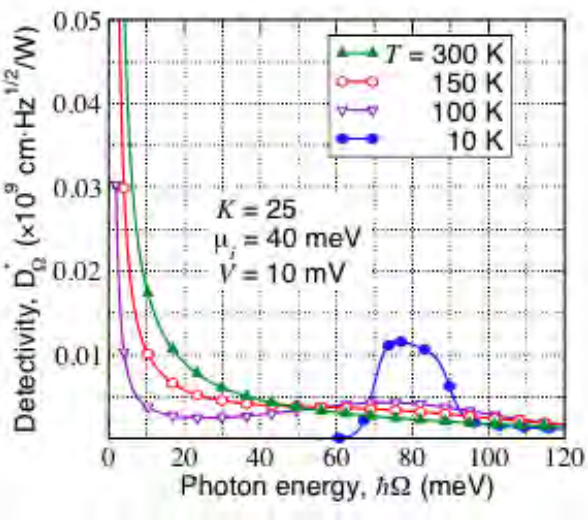

Figure 41. Spectral dependences of the GLPD detectivity at different temperatures (K = 25).

The spectral characteristics depend also on the GL doping level that opens up the prospects of using I-GLPDs in the multi-color systems. The advantages of I-GLPDs under consideration are associated with their sensitivity to the normal incident radiation, weak temperature dependence of the dark current as well as high speed of operation. These devices should be able to operate in the mid-infrared spectral range. We have demonstrated that the I-GLPD characteristics strongly depend on the GL doping level and can be effectively controlled by the bias voltage. The I-GLPD should exhibit a sufficiently high responsivity (about several tenth of A/W) both at low

and room temperatures and a reasonable detectivity at room temperature, surpassing or competing with other IR-photodetectors.

One of the most remarkable features of the I-GLDs is their high-speed operation, ~70 THz, which is associated with short inter-GL tunneling times. Due to the tunneling origin of the photocurrent and dark current, the mid-IR I-GLPDs are expected to achieve a higher speed of operation than the existing photodetectors.

4.6.4 Hot Electron Bolometers based on Transition Metal Dichalcogenides

Graphene is just one of a large number of 2D nanomaterials, which are promising for sensing technologies. In transition metal dichalcogenides, atoms within 2D layers are held by covalent bonds, while different layers are held by weak van der Waals interaction. These 2D materials combine mechanical flexibility and simple processing with high absorption, which may be tuned by varying the number of layers.

2D metal dichalcogenide structures are promising material base for development novel IR detectors based on electron heating in single layer structures. The strong dependence of the electron and IR parameters of the structure on the gate voltage allows for use of the split-gate technique to form nanosensors with unique gate-tunable electronic properties: ultra-small heat capacity, strong electron heating effects, low intrinsic noise, and strong coupling to IR radiation. This advanced fabrication technique can provide THz hot electron nanobolometers with unprecedented low electron heat capacity (~10^{-19} J/K).

The dichalcogenide IR hot electron bolometers may be used as fast direct detectors operating from liquid nitrogen to room temperatures. For example, at the room temperature the small heat capasity leads to small electron-phonon thermal conductance, $G_{e\text{-}ph} = Ce/\tau_\varepsilon \sim 10^{-5}$–$10^{-6}$ W/K (τ_ε is the electron cooling time), which provides strong heating (~ 1K/ μW) and strong photoresponse. The intrinsic noise is given by $NEP = 2T(k_B G_{e\text{-}ph})^{1/2} \sim 3\ 10^{-12}$ W/Hz$^{1/2}$. In combination with low cost and available fabrication technologies these attractive features provide a solid platform for IR sensing applications.

To conclude, results of work are protected by one issued and one pending patent and they are published in four book chapters and twenty six journal papers, also presented at fourty four conferences and resulted in one defended dissertation as listed below. Two more dissertations will be defended (Y.Li and X. Zhang) that are partially based on the results of this work

5. Patents and Publications

PATENTS

1. A. Sergeev, V. Mitin, and G. Strasser, “Vertically correlated clusters of charged quantum dots for optoelectronic devices, and methods of making same,” a regular patent filed PCT/US 13/430,855 on 3/27/2012; the allowance of the patent obtained 1/16/2015.
2. K. A. Sablon, J. W. Little, V. Mitin, A. Sergeev, N. Vagidov, and K. Reinhardt, “Quantum Dot with Built-In Charge Structures with Reduced Wetting Layer for Efficient Photovoltaic Conversion and IR Sensing,” filed as U.S. Provisional Application on July 18, 2011, No. 61-512535 and as a regular patent on 6/30/2012.

PUBLICATIONS

Book chapters

1. V. Mitin, A. Sergeev, L-H. Chien, and N. Vagidov, "Monte-Carlo modeling of electron kinetics in room temperature quantum-dot photodetectors," in *Large-Scale Scientific Computing,* eds. I. Lirkov and S. Margenov, Spinger Berlin / Heidelberg, 2010, pp. 403-410.
2. K. A. Sablon, V. Mitin, J. W. Little, A. Sergeev and N. Vagidov, "Quantum dots with built-in charge for enhancing quantum dot solar cells and infrared photodetectors," Chapter 13 in *Quantum Dot Devices,* Lecture Notes in Nanoscale Science and Technology, Vol. **13**, ed. Zhiming Wang, Springer, 2012.
3. V. Ryzhii, N. Ryabova, M. Ryzhii, V. Mitin, and T. Otsuji, "Concepts of terahertz and infrared photodiodes and phototransistors based on graphene structures," Chapter 6.2, pp. 197-205, in *Frontier Techno Series* No.**17**, *Application of state-of-the-art technology and the spread of graphene*, 2012, SBN978-4-902410-24-2.
4. A. Sergeev, N. Vagidov, V. Mitin, and K. Sablon, "Charged quantum dots for high efficiency photovoltaics and IR sensing," in *Future Trends in Microelectronics*, editors S. Luryi, J. Xu, and A. Zaslavsky, Wiley-IEEE Press, 2013, pp.244-253.

Journal papers

1. L.-H. Chien, A. Sergeev, V. Mitin, N. Vagidov, and S. Oktyabrsky, "Nanostructures with quantum dot clusters: Long photocarrier lifetime," *Nanoscience and Nanotechnology Letters* **2**, 1 (2010).
2. Li-Hsin Chien, A. Sergeev, V. Mitin, S. Oktyabrsky, "Quantum dot photodetectors based on structures with collective potential barriers", in Quantum Sensing and Nanophotonic Devices VII, Manijeh Razeghi; Rengarajan Sudharsanan; Gail J. Brown, Editors, *Proceedings of SPIE* Vol. 7608 (SPIE, Bellingham, WA 2010), 760826.
3. V. Mitin, A. Antipov, A. Sergeev, N. Vagidov, D. Eason, and G. Strasser, "Quantum dot infrared photodetectors: Photoresponse enhancement due to potential barriers," *Nanoscale Research Letters,* **6**, 21 (2011).
4. L.-H. Chien, A. Sergeev, N. Vagidov, V. Mitin, and S. Birner, "Electron heating in quantum-dot structures with collective potential barriers," *International Journal of High Speed Electronics and Systems*, 20, 143-152 (2011).
5. K. Sablon, A. Sergeev, N. Vagidov, A. Antipov, J.W. Little, and V. Mitin," Effective harvesting, detection, and conversion of IR radiation due to quantum dots with built-incharge," *Nanoscale Research Letters* 6, 584 (2011).
6. M. Ryzhii, T. Otsuji, V. Mitin, V. Ryzhii, "Characteristics of p-i-n Terahertz and Infrared Photodiodes Based on Multiple Graphene Layer Structures", *Japanese Journal of Appl. Phys.* 50, 070117, 2011.
7. K. A. Sablon, J. W. Little, V. Mitin, A. Sergeev, N. Vagidov, K. Reinhardt, "High-efficiency quantum dot solar cells due to inter-dot n-doping", in Next Generation (Nano) Photonic and

Cell Technologies for Solar Energy Conversion II, Loucas Tsakalakos, Editors, Proceedings of SPIE Vol. 8111 (SPIE, Bellingham, WA 2011), 81110H.

8. A. Antipov, M. Bell, M. Yasar, V. Mitin, W. Scharmach, M. Swihart, A.Verevkin, and A. Sergeev**,** "Luminescence of colloidal CdSe/ZnS nanoparticles: High sensitivity to solvent phase transitions," *Nanoscale Research Letters* **6**, 142 (2011).
9. V. Ryzhii, M. Ryzhii, N. Ryabova, V. Mitin, T. Otsuji, "Terahertz and infrared detectors based on graphene structures", , Infrared Phys. and Tech. 54, 302-305, 2011.
10. J. K. Choi, N. Vagidov, A. Sergeev, S. Kalchmair, G. Strasser, F. T. Vasko, and V. V. Mitin, Asymmetrically doped GaAs/AlGaAs double-quantum-well structure for voltage-tunable IR detection, *Jap. J. Appl. Phys.* **51**, 074004, 2012.
11. S. Oktyabrsky, V.E. Tokranov, M. Yakimov, A.V. Sergeev, and V.V. Mitin, "Nanoengineered quantum dot medium for space optoelectronic devices", in Nanophotonics and Macrophotonics for Space Environments VI, Edward W. Taylor; David A. Cardimona, Editors, Proceedings of SPIE Vol. **8519** (SPIE, Bellingham, WA 2012), 851907.
12. F. Vasko and V. Mitin, "Superlattice formed by quantum-dot sheets: Density of states and infrared absorption", *Physical Review B* **85**, 235321, 2012.
13. V. Ryzhii, T. Otsuji, N. Ryabova, M. Ryzhii, V. Mitin and V. Karasik, "Concept of infrared photodetector based on graphene-graphene nanoribbon structure", *Infrared Phys. and Technol.*, Vol. **59**, pp. 137-141, 2013.
14. V. Ryzhii, T. Otsuji, M. Ryzhii, N. Ryabova, S. O. Yurchenko, V. Mitin and M. S. Shur, "Graphene terahertz uncooled bolometers," *J. Phys. D: Appl. Phys.*, **46**, 065102, 2013.
15. V. L. Semenenko, V. G. Leiman, A. V. Arsenin, V. Mitin, M. Ryzhii, T. Otsuji, and V Ryzhii, "Effect of self-consistent electric field on characteristics of graphene p-i-n tunneling transit-time diodes," *J. Appl. Phys.*, Vol. **113**, pp. 024503-1-7, 2013.
16. F. T. Vasko, V. V. Mitin, V. Ryzhii and T. Otsuji, "Interplay of intra- and interband absorption in a disordered graphene," *Phys. Rev. B* **86**, 235424 (1-7), 2012.
17. F. T. Vasko and V. V. Mitin, "Diffusion of photoexcited carriers in graphene," *Appl. Phys. Lett.* **101**, 151115 (1-4), 2012.
18. F. T. Vasko, and V. Mitin, "Electronic states in heterostructures formed by ultranarrow layers", *J. Phys.: Condens. Matter* **24**, 445010 (1-8), 2012.
19. V. Mitin, A. Sergeev, N. Vagidov, and S. Birner, "Improvement of QDIP performance due to quantum dots with built-in charge," *Infrared Physics & Technology* **59**, 84-88 (2013).
20. V.V. Mitin, Jae Kyu Choi, G. Thomain, K.A. Sablon, S. Oktyabrsky, N.Z. Vagidov, and A.V. Sergeev, "Charge redistribution in adaptable quantum-dot and quantum-well nanomaterials for infrared sensing ", in Micro- and Nanotechnology Sensors, Systems, and Applications V, Thomas George; M. Saif Islam; Achyut K. Dutta, Editors, *Proceedings of SPIE* Vol. **8725** (SPIE, Bellingham, WA 2013), 87250D.
21. M. Yakimov, A. Sergeev, V. Pogrebnyak, A. Varghese, V. E. Tokranov, G. Thomain, N. Vagidov, V. Mitin, and S. Oktyabrsky, "Engineering of absorbing medium for quantum dot infrared photodetectors", in Nanophotonics and Macrophotonics for Space Environments

VII, Edward W. Taylor; David A. Cardimona, Editors, Proceedings of SPIE Vol. 8876 (SPIE, Bellingham, WA 2013), 88760V.

22. V. Ryzhii, A. Satou, T. Otsuji, M. Ryzhii, V. Mitin and M.S. Shur, "Dynamic effects in double graphene-layer structures with inter-layer resonant-tunnelling negative conductivity," *J. Phys. D: Appl. Phys.* Vol. **46**, 315107, 2013.
23. V. Ryzhii, T. Otsuji, V. Ya. Aleshkin, A. A. Dubinov, M. Ryzhii, V. Mitin, and M. S. Shur, "Voltage-tunable terahertz and infrared photodetectors based on double-graphene-layer structures", *Appl. Phys. Let.* Vol. **104**, 163505, 2014.
24. D. Svintsov, T. Otsuji, V. Mitin, M. S. Shur, and V. Ryzhii, "Negative terahertz conductivity in disordered graphene bilayers with population Inversion", *Appl. Phys. Lett*. **106**, 113501 1-5 (2015); doi: 10.1063/1.4915314.
25. V. Ryzhii, A. Satou, T. Otsuji, M. Ryzhii, V. Mitin, and M. S. Shur, "Graphene vertical hot-electron terahertz detectors", J. Appl. Phys. 116, 114504 (2014).
26. V. Ryzhii, T. Otsuji, M. Ryzhii, V. Ya. Aleshkin,A. A. Dubinov, D. Svintsov, V. Mitin, and M.S. Shur, "Graphene vertical cascade interband terahertz and infrared photodetectors", *2D Mater*. 2 (2015) 025002 doi:10.1088/2053-1583/2/2/025002.

Presentations and conference publications

1. A. Sergeev, N. Vagidov, and V. Mitin, "Nanoscale Engineering of Photoelectron Kinetics in Quantum Dot Structures," *APS March Meeting* 21-25, 2011, Texas, Dallas, book of abstracts K1.00001.
2. A. Sergeev, M. Reizer, and V. Mitin, "Concentration Dependence of the Electron-Phonon Coupling from Metals to Semiconductors," *APS March Meeting* 21-25, 2011, Texas, Dallas, book of abstracts X22.00007.
3. J. K. Choi, D. Eason, G. Strasser, N. Vagidov, V. Mitin, "Voltage Tunable Multicolor GaAs/AlGaAs Coupled Quantum Well Infrared Photodetector," *APS March Meeting* 21-25, 2011, Texas, Dallas, book of abstracts S1.00232.
4. M. Ryzhii, V. Ryzhii, T. Otsuji, and V. Mitin, "Terahertz and Infrared Detectors Based on Multiple-graphene Layers with p-i-n Junctions: Device Model and Characteristics," Invited talk at the *Progress In Electromagnetics Research Symposium* (PIERS-2011), March 20-23, 2011, Marrakesh, Morocco, Session 3P2.
5. V. Mitin, A. Sergeev, N. Vagidov, S. Oktyabrsky, and M. Yakimov, "Advanced Quantum Dot Structures with Manageable Photoelectron Kinetics," invited talk at the 2011 *Villa Conference on Interaction among Nanostructure*s (VCIAN), April 21-25, 2011, Las Vegas, NV.
6. A. Sergeev, M. Reizer, V. Mitin, "Nanoscale Engineering of Electron Interactions: Novel Phenomena and Advanced Devices," invited talk at the 2011 *Villa Conference on Interaction among Nanostructures* (VCIAN), April 21-25, 2011, Las Vegas, NV.
7. V. Mitin, "Effective Conversion of IR Radiation in Quantum Dot Solar Cells Due to Inter-Dot n-Doping," invited talk at the Workshop *Materials and Plasmonics: Novel Materials,*

Design, and Applications, May 16-17, 2011, Buffalo, NY.

8. V. Mitin, A. Sergeev, N. Vagidov, K. A. Sablon, and J. W. Little, "Quantum Dot IR Photodetectors and Solar Cells Enhanced by Built-in-Charge,"Proceedings of the *15th International Conference on Narrow Gap Systems* (NGS15), August 1-5, Blacksburg, Virginia, USA, and AIP Conf. Proc. 1416, 52-55, 2011.
9. F. T. Vasko and V. Mitin, "Generation-Recombination Processes via Acoustic Phonons in a Disorded Graphene", Proceedings of the *15th International Conference on Narrow Gap Systems* (NGS15), August 1-5, Blacksburg, Virginia, USA, and AIP Conf. Proc. 1416, 181-183, 2011.
10. V. Ryzhii, M. Ryzhii, A. Satou, T. Otsuji, and V. Mitin, "Nonequilibrium Carriers and Phonons in Optically Excited Graphene: Heating and Cooling," Proceedings of the *17th International Conference on Electron Dynamics in Semiconductors, Optoelectronics and Nanostructures* (EDISON 17), August 7-12, 2011, Santa Barbara, California, USA, pp. 173-174.
11. V. Mitin, K. A. Sablon, J. W. Little, A. Sergeev, N. Vagidov, and K. Reinhardt, "Solar Cells and Photodetectors: High Performance Provided by Built-in-Dot Charge", Proceedings of the 17th *International Conference on Electron Dynamics in Semiconductors, Optoelectronics and Nanostructures* (EDISON 17), August 7-12, 2011, Santa Barbara, California, USA, pp. 50-51.
12. V. Ryzhii, M. Ryzhii, A. Dubinov, V. Aleshkin, V. Mitin, M. Shur, A. Satou, S. A. B. Tombet and T. Otsuji, "Concepts of Terahertz and Infrared Devices Based on Graphene Structures," invited talk at Proceedings of *the 36th International Conference on Infrared, Millimeter and Terahertz Waves* (IRMMW), October 2-7, 2011, Houston, Texas, USA, Proceedings Tu3C.1.
13. V. Mitin, "High Performance Solar Cells and Photodetectors on Quantum Dot Structures with Built-in-Charge," invited talk at the BIT's 1st Annual World Congress of Nano-S & T, October 23-26, 2011, Dalian, China.
14. N. Vagidov, A. Sergeev, A. Antipov, K. Sablon, J. Little, and V. Mitin,"Quantum-Dot Nanostructures for Effective Harvesting, Detection, and Conversion of IR Radiation," *APS March Meeting*, February 27 – March 2, 2012, Boston, Massachusetts, book of abstracts A33.11.
15. F. Vasko, V. Mitin, and A. Sergeev, "Effects of Disorder on Recombination and Relaxation Processes via Acoustic Phonons in Graphene," *APS March Meeting*, February 27 – March 2, 2012, Boston, Massachusetts, book of abstracts D11.10.
16. V. Mitin and F. Vasko, "Superlattice Formed by Quantum Dot Sheets: Density of States and IR Absorption," *APS March Meeting*, February 27 – March 2, 2012, Boston, Massachusetts, book of abstracts S1.149.
17. J. K. Choi, N. Vagidov, A. Sergeev, G. Strasser, F. Vasko, and V. Mitin, "Voltage-Tunable IR Photodetector Based on Asymmetrically Doped Coupled Quantum Wells", *APS March Meeting*, February 27 – March 2, 2012, Boston, Massachusetts, book of abstracts S1.150.
18. F.T. Vasko and V. Mitin, "Generation-Recombination Processes via Acoustic Phonons and Transient Population Inversion in Graphene," invited talk at the *Japan-Russia-USA*

Symposium on Modeling of Graphene Terahertz, Nano-Mechanical, and Acousto-Optical Devices, Aizu-Wakamatsu, Japan, March 7-10, 2012, book of abstracts.

19. V. Mitin and F. Vasko, "Superlattice Formed by Quantum Dot Sheets: Density of States and IR Absorption", *NANOSMAT-USA International Conference on Surfaces, Coatings, and Nano-Structured Materials*, March 27-30, 2012, Tampa, FL.
20. V. Mitin and F. Vasko, "Nonequilibrium Carriers in Graphene: Diffusion, Recombination, and Transient Population Inversion," invited talk at the *US-Japan TeraNano Workshop on Nanophotonics and Nanoelectronics*, May 11, 2012, Buffalo, NY.
21. V. Ryzhii, N. Ryabova, M. Ryzhii, T. Otsuji, V. Mitin, and V.E. Karasik, "Concept of Terahertz and Infrared Detectors Based on Graphene Strusctures," *Quantum Structure Infrared Photodetector International Conference*, QSIP 2012, June 17-23, 2012, Cargese, Corsica, France, Book of abstracts p. 33, and the Proceedings of the International Conferenece on Quantum Structure Infrared Photodetector International Conference (QSIP) 2012, editors Ph. Bois and S.D. Gunapala, Elsevier, pp. 137-141.
22. S. Oktyabrsky, V.E. Tokranov, M. Yakimov, A.V. Sergeev, Vladimir V. Mitin, "Nanoengineered quantum dot medium for space optoelectronic devices,", Keynote Presentation, Paper 8519-6 at the SPIE Optical Engineering + Applications, 12 - 16 August 2012. San Diego, CA and paper in SPIE Optics + Photonics Proc. SPIE 8519, 851907 (2012).
23. A. Sergeev, N. Vagidov, V. Mitin, K. Sablon, and J. Little, "Nanoscale engineering of photoelectron processes by charging quantum dots", IEEE NANO 2012, *12th International Conference on Nanotechnology*, 20 - 23 August 2012, Birmingham, UK, book of abstracts.
24. V. Mitin, A. Sergeev, N. Vagidov, K. Sablon, M. Yakimov, and S. Oktyabrsky, "Photoelectron Kinetics in Nanomaterials with Charged Dots: Physics and Applications", Invited talk at the *7th International Cnference on Surfaces, Coatings and Nanostructured Materials* (Nanosmat), 18-21 September 2012, Prague, Technical Program, p.14, Talk Nano-108.
25. V. Ryzhii, T. Otsuji, M. Ryzhii, V. Mitin, M.S. Shur, "Graphene-based infrared and terahertz detectors: Concepts, features, and comparison," invited talk at *Int. Conf. on Micro and Nanoelectronics* (ICMNE), L2-01, Moscow, Russia, Oct. 1-5, 2012.
26. V. Mitin, F. T. Vasko, V. Ryzhii, and T. Otsuji, "Interplay of Intraband and Interband Absorption in a Disordered Graphene," *3rd International Sympposium on Graphene Devices* (ISGD-2012), November 5-9, 2012, Synchrotron SOLEIL, Saint-Aubin, France, book of abstracts, OC-05, p. 16.
27. "V. Mitin, K. Sablon, J. Little, A. Sergeev, and N. Vagidov, "Nanomaterials with Charged Quantum Dots for Conversion and Sensing Applications," invited talk at 2012 MRS Fall Meeting, November 25-30, 2012, Boston, MA, Talk E8.03*, p. 160 of the Program.
28. V. Mitin, F. T. Vasko, V. Ryzhii, and T. Otsuji, "Distinctiveness of Non-equilibrium Carriers in Disordered Graphene," *3rd International Simposium on Terahertz Nanoscience*, December 10-12, 2012, Honolulu, Hawaii, book of abstracts, p. 20.

29. A. Satou, V. Ryzhii, F.T. Vasko, V.V. Mitin, T. Otsuji, "Numerical simulation of terahertz plasmons in gated graphene structures," *SPIE Photonics West*, 8624-37, San Francisco, CA, Feb. 6, 2013, book of abstracts.
30. G. Thomain, V. Mitin, V.Pogrebnyak, and A. Sergeev, "Effect of doping on performance of IR quantum dot photodetector," *APS March Meeting* 2013, March 18–22, 2013; Baltimore, Maryland, book of abstracts.
31. A. Sergeev, M. Reizer, and V. Mitin, "Electron relaxation via interaction with optical phonons in disordered metals and semiconductors," *APS March Meeting*, March 18–22, 2013; Baltimore, Maryland.
32. V. Ryzhii, T. Otsuji, M. Ryzhii, V. Mitin and M.S. Shur, "Terahertz detectors and photomixers based on double-graphene-layer structures utilizing plasma resonances," *International Workshop on Optical Terahertz Science and Technology* 2013, Kyoto, Japan, April 1-5, 2013, book of abstracts TH3-04.
33. V. Mitin, N. Vagidov, K. Sablon, and A. Sergeev, "Adaptive quantum-dot based materials for detection and broad band photovoltaic conversion," invited talk at the *SPIE Defense, Security and Sensing* 2013, April 28-May 3, 2013, Baltimore, MD.
34. V. Mitin, G. Thomain, N. Vagidov, A. Sergeev, M. Yakimov, and S. Oktyabrsky, "Adaptable quantum dot nanomaterials for advanced sensing,", International Conference on Materials and Applications for Sensors and Transducers (IC-MAST 2013), Prague, Czech Republic, September 13-17, 2013.
35. V. Mitin, A. Sergeev, N. Vagidov, and K. Sablon, "Nanomaterials with charged quantum dots for broad band solar energy conversion and advanced sensing," *Nano and Giga Challenges in Electronics, Photonics and Renewable Energy: From Materials to Devices to System Architecture*, Symposium and Spring School, Phoenix, Arizona, March 10-14, 2014.
36. V. Mitin, V. Ryzhii, T. Otsuji, V. Ya. Aleshkin, A. A. Dubinov, M. Ryzhii, and M. S. Shur, "High sensitivity terahertz and infrared detectors based on double-graphene-layer structures," *International Conference on Materials and Applications for Sensors and Transducers* (IC-MAST 2014), Bilbao, Spain, June 8-11, 2014, book of abstracts.
37. "Nanomaterials with manageable charge of nanoblocks for adaptive sensing", APS March Meeting 2014, March 3–7, 2014; Denver, CO, book of abstracts.
38. G. Thomain, X. Zhang, N. Vagidov, V. Mitin, and A. Sergeev, "Challenges in quantum dot IR/THz sensing technologies," *The 3rd RJUS Symposium on Fundamental & Applied Problems of Terahertz Devices & Technologies*, June 17-20, 2014, University at Buffalo, NY, USA.
39. A. Sergeev, V. Mitin, N. Vagidov, K. Sablon, J. Little, K. Reinhardt, "Adaptable quantum dot nanomaterials with controllable kinetics," *International Conference on Physics of Semiconductors*, ICPS 2014, August 10-15, Austin, TX, USA.
40. T. Otsuji, V. Ryzhii, S. Boubanga Tombet, T. Watanabe, A. Satou, M. Ryzhii, A. Dubinov, V. Ya Aleshkin, V. Popov, V. Mitin, and M.S. Shur, "Graphene plasmonic heterostructures for new typse of terahertz lasers", SPIE Optics + Photonics 2014, Conf. 9199, Terahertz Emission, Detection and Applications V, 9199-14, San Diego, CA, USA, 17 Aug. 2014. (invited); Proc. SPIE, Vol. 9199, pp. 91990F-1-10

41. T. Otsuji, T. Watanabe, A. Satou, S. A. Boubanga-Tombet, A. Dubinov, V. V. Popov, V. Mitin, V. Ryzhii, “Giant Terahertz Gain by Excitation of Surface Plasmon Polaritons in Optically Pumped Graphene”, ISGD: 4th International Symposium on Graphene Devices, A4.05, Seattle, USA, 25 Sept. 2014. (invited)
42. A. Sergeev and V. Mitin, “Nanoscale Engineering of Energy Transfer in Optoelectronic Materials for Sensing and Conversion,” invited talk at Functional Materials Division, Materials and Manufacturing Directorate of AFOSR, Dayton, October 28, 2014.
43. X. Zhang, A. Sergeev. V. Mitin, K. Sablon, M. Yakimov, and S. Oktyabrsky, “Adaptable Quantum Dot Nanomaterials for IR Sensing”, *APS March Meeting 2015*, March 2-6, 2015; San Antonio, Texas, Bulletin of the American Physical Society, V. 60, No. 1, V1.00198.
44. V. Mitin, A. Sergeev, X. Zhang, and T. Yore, “Reconfigurable nanomaterials for adaptive sensing: Electric and optical control of nanoscale potential profile”, Advanced Research Workshop "Future Trends in Microelectronics: Journey into the Unknown", June 21-26, 2015 Mallorca, Spain, book of abstract, paper to be published in proceedings.

Thesis/Dissertations

1. G. Thomain, “Nanoscale engineering of photoelectron processes for infrared detection,” Ph.D. Dissertation, July 2014, State University of New York at Buffalo, ProQuest, UMI Dissertations Publishing, 2014. 3640883

1.

1. Report Type

Final Report

Primary Contact E-mail

Contact email if there is a problem with the report.

vmitin@buffalo.edu

Primary Contact Phone Number

Contact phone number if there is a problem with the report

716-645-1036

Organization / Institution name

University at Buffalo

Grant/Contract Title

The full title of the funded effort.

ADAPTIVE IR SENSING BASED ON ADVANCED NANOSTRUCTURES WITH TUNABLE KINETICS

Grant/Contract Number

AFOSR assigned control number. It must begin with "FA9550" or "F49620" or "FA2386".

FA9550-10-1-0391

Principal Investigator Name

The full name of the principal investigator on the grant or contract.

Vladimir Mitin

Program Manager

The AFOSR Program Manager currently assigned to the award

Dr. Kenneth C. Goretta

Reporting Period Start Date

08/01/2010

Reporting Period End Date

07/31/2015

Abstract

The project addressed development of novel reconfigurable nanomaterials and adaptive IR detectors for third generation infrared imaging systems. The research program focused on design on advanced quantum dot (QD) and quantum well (QW) nanostructures and graphene-based nanomaterials with tunable kinetics of photoelectrons.

The research program established scientific, engineering, and technological basis for further development of IR nanomaterials with nanoscale potential profile that can be effectively controlled by voltage bias and/or optical bias. While currently optoelectronic devices are based on the structures with potential barriers changing in one and/or two dimensions, the innovative approach is based on the novel paradigm of 3D nanoscale potential, which strongly enhances functionality of materials and structures. Moreover, bias-tunable nanoscale profile provides fast and efficient control of all optoelectronic properties of novel reconfigurable nanomaterials. Achieved tunable and sensing functionalities provide fast and effective control of the major optoelectronic properties including photocarrier lifetime, electron transport, spectral characteristics, noise parameters, and coupling to electromagnetic radiation.

We also demonstrated that the single graphene layer, graphene bi-layers, graphene nano-ribbon, and multiple graphene layer structures opens up prospects of further enhancement of capabilities of graphene-based optoelectronic devices, in particular, IR detectors and emitters.

Distribution Statement

This is block 12 on the SF298 form.

Distribution A - Approved for Public Release

Explanation for Distribution Statement

If this is not approved for public release, please provide a short explanation. E.g., contains proprietary information.

SF298 Form

Please attach your SF298 form. A blank SF298 can be found here. Please do not password protect or secure the PDF The maximum file size for an SF298 is 50MB.

AFD-070820-035-for final report VM+.pdf

Upload the Report Document. File must be a PDF. Please do not password protect or secure the PDF . The maximum file size for the Report Document is 50MB.

Report to Ken final 2015-08-22.pdf

Upload a Report Document, if any. The maximum file size for the Report Document is 50MB.

Archival Publications (published) during reporting period:

PUBLICATIONS

Book chapters

1. V. Mitin, A. Sergeev, L-H. Chien, and N. Vagidov, “Monte-Carlo modeling of electron kinetics in room temperature quantum-dot photodetectors,” in Large-Scale Scientific Computing, eds. I. Lirkov and S. Margenov, Spinger Berlin / Heidelberg, 2010, pp. 403-410.
2. K. A. Sablon, V. Mitin, J. W. Little, A. Sergeev and N. Vagidov, “Quantum dots with built-in charge for enhancing quantum dot solar cells and infrared photodetectors,” Chapter 13 in Quantum Dot Devices, Lecture Notes in Nanoscale Science and Technology, Vol. 13, ed. Zhiming Wang, Springer, 2012.
3. V. Ryzhii, N. Ryabova, M. Ryzhii, V. Mitin, and T. Otsuji, “Concepts of terahertz and infrared photodiodes and phototransistors based on graphene structures,” Chapter 6.2, pp. 197-205, in Frontier Techno Series No.17, Application of state-of-the-art technology and the spread of graphene, 2012, SBN978-4-902410-24-2.
4. A. Sergeev, N. Vagidov, V. Mitin, and K. Sablon, “Charged quantum dots for high efficiency photovoltaics and IR sensing,” in Future Trends in Microelectronics, editors S. Luryi, J. Xu, and A. Zaslavsky, Wiley-IEEE Press, 2013, pp.244-253.

Journal papers

1. L.-H. Chien, A. Sergeev, V. Mitin, N. Vagidov, and S. Oktyabrsky, “Nanostructures with quantum dot clusters: Long photocarrier lifetime,” Nanoscience and Nanotechnology Letters 2, 1 (2010).
2. Li-Hsin Chien, A. Sergeev, V. Mitin, S. Oktyabrsky, "Quantum dot photodetectors based on structures with collective potential barriers", in Quantum Sensing and Nanophotonic Devices VII, Manijeh Razeghi; Rengarajan Sudharsanan; Gail J. Brown, Editors, Proceedings of SPIE Vol. 7608 (SPIE, Bellingham, WA 2010), 760826.
3. V. Mitin, A. Antipov, A. Sergeev, N. Vagidov, D. Eason, and G. Strasser, “Quantum dot infrared photodetectors: Photoresponse enhancement due to potential barriers,” Nanoscale Research Letters, 6, 21 (2011).
4. L.-H. Chien, A. Sergeev, N. Vagidov, V. Mitin, and S. Birner, “Electron heating in quantum-dot structures with collective potential barriers,” International Journal of High Speed Electronics and Systems, 20, 143-152 (2011).
5. K. Sablon, A. Sergeev, N. Vagidov, A. Antipov, J.W. Little, and V. Mitin,” Effective harvesting, detection, and conversion of IR radiation due to quantum dots with built-incharge,” Nanoscale Research Letters 6, 584 (2011).
6. M. Ryzhii, T. Otsuji, V. Mitin, V. Ryzhii, “Characteristics of p-i-n Terahertz and Infrared Photodiodes Based on Multiple Graphene Layer Structures”, Japanese Journal of Appl. Phys. 50, 070117, 2011.
7. K. A. Sablon, J. W. Little, V. Mitin, A. Sergeev, N. Vagidov, K. Reinhardt, "High-efficiency quantum dot solar cells due to inter-dot n-doping", in Next Generation (Nano) Photonic and Cell Technologies for Solar

Energy Conversion II, Loucas Tsakalakos, Editors, Proceedings of SPIE Vol. 8111 (SPIE, Bellingham, WA 2011), 81110H.
8. A. Antipov, M. Bell, M. Yasar, V. Mitin, W. Scharmach, M. Swihart, A.Verevkin, and A. Sergeev, “Luminescence of colloidal CdSe/ZnS nanoparticles: High sensitivity to solvent phase transitions,” Nanoscale Research Letters 6, 142 (2011).
9. V. Ryzhii, M. Ryzhii, N. Ryabova, V. Mitin, T. Otsuji, “Terahertz and infrared detectors based on graphene structures”, , Infrared Phys. and Tech. 54, 302-305, 2011.
10. J. K. Choi, N. Vagidov, A. Sergeev, S. Kalchmair, G. Strasser, F. T. Vasko, and V. V. Mitin, Asymmetrically doped GaAs/AlGaAs double-quantum-well structure for voltage-tunable IR detection, Jap. J. Appl. Phys. 51, 074004, 2012.
11. S. Oktyabrsky, V.E. Tokranov, M. Yakimov, A.V. Sergeev, and V.V. Mitin, "Nanoengineered quantum dot medium for space optoelectronic devices", in Nanophotonics and Macrophotonics for Space Environments VI, Edward W. Taylor; David A. Cardimona, Editors, Proceedings of SPIE Vol. 8519 (SPIE, Bellingham, WA 2012), 851907.
12. F. Vasko and V. Mitin, “Superlattice formed by quantum-dot sheets: Density of states and infrared absorption”, Physical Review B 85, 235321, 2012.
13. V. Ryzhii, T. Otsuji, N. Ryabova, M. Ryzhii, V. Mitin and V. Karasik, “Concept of infrared photodetector based on graphene-graphene nanoribbon structure”, Infrared Phys. and Technol., Vol. 59, pp. 137-141, 2013.
14. V. Ryzhii, T. Otsuji, M. Ryzhii, N. Ryabova, S. O. Yurchenko, V. Mitin and M. S. Shur, “Graphene terahertz uncooled bolometers,” J. Phys. D: Appl. Phys., 46, 065102, 2013.
15. V. L. Semenenko, V. G. Leiman, A. V. Arsenin, V. Mitin, M. Ryzhii, T. Otsuji, and V Ryzhii, “Effect of self-consistent electric field on characteristics of graphene p-i-n tunneling transit-time diodes,” J. Appl. Phys., Vol. 113, pp. 024503-1-7, 2013.
16. F. T. Vasko, V. V. Mitin, V. Ryzhii and T. Otsuji, “Interplay of intra- and interband absorption in a disordered graphene,” Phys. Rev. B 86, 235424 (1-7), 2012.
17. F. T. Vasko and V. V. Mitin, “Diffusion of photoexcited carriers in graphene,” Appl. Phys. Lett. 101, 151115 (1-4), 2012.
18. F. T. Vasko, and V. Mitin, “Electronic states in heterostructures formed by ultranarrow layers”, J. Phys.: Condens. Matter 24, 445010 (1-8), 2012.
19. V. Mitin, A. Sergeev, N. Vagidov, and S. Birner, “Improvement of QDIP performance due to quantum dots with built-in charge,” Infrared Physics & Technology 59, 84-88 (2013).
20. V.V. Mitin, Jae Kyu Choi, G. Thomain, K.A. Sablon, S. Oktyabrsky, N.Z. Vagidov, and A.V. Sergeev, "Charge redistribution in adaptable quantum-dot and quantum-well nanomaterials for infrared sensing ", in Micro- and Nanotechnology Sensors, Systems, and Applications V, Thomas George; M. Saif Islam; Achyut K. Dutta, Editors, Proceedings of SPIE Vol. 8725 (SPIE, Bellingham, WA 2013), 87250D.
21. M. Yakimov, A. Sergeev, V. Pogrebnyak, A. Varghese, V. E. Tokranov, G. Thomain, N. Vagidov, V. Mitin, and S. Oktyabrsky, "Engineering of absorbing medium for quantum dot infrared photodetectors", in Nanophotonics and Macrophotonics for Space Environments VII, Edward W. Taylor; David A. Cardimona, Editors, Proceedings of SPIE Vol. 8876 (SPIE, Bellingham, WA 2013), 88760V.
22. V. Ryzhii, A. Satou, T. Otsuji, M. Ryzhii, V. Mitin and M.S. Shur, “Dynamic effects in double graphene-layer structures with inter-layer resonant-tunnelling negative conductivity,” J. Phys. D: Appl. Phys. Vol. 46, 315107, 2013.
23. V. Ryzhii, T. Otsuji, V. Ya. Aleshkin, A. A. Dubinov, M. Ryzhii, V. Mitin, and M. S. Shur, “Voltage-tunable terahertz and infrared photodetectors based on double-graphene-layer structures”, Appl. Phys. Let. Vol. 104, 163505, 2014.
24. D. Svintsov, T. Otsuji, V. Mitin, M. S. Shur, and V. Ryzhii, “Negative terahertz conductivity in disordered graphene bilayers with population Inversion”, Appl. Phys. Lett. 106, 113501 1-5 (2015); doi: 10.1063/1.4915314.
25. V. Ryzhii, A. Satou, T. Otsuji, M. Ryzhii, V. Mitin, and M. S. Shur, “Graphene vertical hot-electron terahertz detectors”, J. Appl. Phys. 116, 114504 (2014).
26. V. Ryzhii, T. Otsuji, M. Ryzhii, V. Ya. Aleshkin,A. A. Dubinov, D. Svintsov, V. Mitin, and M.S. Shur, “Graphene vertical cascade interband terahertz and infrared photodetectors”, 2D Mater. 2 (2015) 025002

doi:10.1088/2053-1583/2/2/025002.

Presentations and conference publications

1. A. Sergeev, N. Vagidov, and V. Mitin, “Nanoscale Engineering of Photoelectron Kinetics in Quantum Dot Structures,” APS March Meeting 21-25, 2011, Texas, Dallas, book of abstracts K1.00001.
2. A. Sergeev, M. Reizer, and V. Mitin, “Concentration Dependence of the Electron-Phonon Coupling from Metals to Semiconductors,” APS March Meeting 21-25, 2011, Texas, Dallas, book of abstracts X22.00007.
3. J. K. Choi, D. Eason, G. Strasser, N. Vagidov, V. Mitin, “Voltage Tunable Multicolor GaAs/AlGaAs Coupled Quantum Well Infrared Photodetector,” APS March Meeting 21-25, 2011, Texas, Dallas, book of abstracts S1.00232.
4. M. Ryzhii, V. Ryzhii, T. Otsuji, and V. Mitin, “Terahertz and Infrared Detectors Based on Multiple-graphene Layers with p-i-n Junctions: Device Model and Characteristics,” Invited talk at the Progress In Electromagnetics Research Symposium (PIERS-2011), March 20-23, 2011, Marrakesh, Morocco, Session 3P2.
5. V. Mitin, A. Sergeev, N. Vagidov, S. Oktyabrsky, and M. Yakimov, “Advanced Quantum Dot Structures with Manageable Photoelectron Kinetics,” invited talk at the 2011 Villa Conference on Interaction among Nanostructures (VCIAN), April 21-25, 2011, Las Vegas, NV.
6. A. Sergeev, M. Reizer, V. Mitin, “Nanoscale Engineering of Electron Interactions: Novel Phenomena and Advanced Devices,” invited talk at the 2011 Villa Conference on Interaction among Nanostructures (VCIAN), April 21-25, 2011, Las Vegas, NV.
7. V. Mitin, “Effective Conversion of IR Radiation in Quantum Dot Solar Cells Due to Inter-Dot n-Doping,” invited talk at the Workshop Materials and Plasmonics: Novel Materials, Design, and Applications, May 16-17, 2011, Buffalo, NY.
8. V. Mitin, A. Sergeev, N. Vagidov, K. A. Sablon, and J. W. Little, “Quantum Dot IR Photodetectors and Solar Cells Enhanced by Built-in-Charge,”Proceedings of the 15th International Conference on Narrow Gap Systems (NGS15), August 1-5, Blacksburg, Virginia, USA, and AIP Conf. Proc. 1416, 52-55, 2011.
9. F. T. Vasko and V. Mitin, “Generation-Recombination Processes via Acoustic Phonons in a Disorded Graphene”, Proceedings of the 15th International Conference on Narrow Gap Systems (NGS15), August 1-5, Blacksburg, Virginia, USA, and AIP Conf. Proc. 1416, 181-183, 2011.
10. V. Ryzhii, M. Ryzhii, A. Satou, T. Otsuji, and V. Mitin, “Nonequilibrium Carriers and Phonons in Optically Excited Graphene: Heating and Cooling,” Proceedings of the 17th International Conference on Electron Dynamics in Semiconductors, Optoelectronics and Nanostructures (EDISON 17), August 7-12, 2011, Santa Barbara, California, USA, pp. 173-174.
11. V. Mitin, K. A. Sablon, J. W. Little, A. Sergeev, N. Vagidov, and K. Reinhardt, “Solar Cells and Photodetectors: High Performance Provided by Built-in-Dot Charge”, Proceedings of the 17th International Conference on Electron Dynamics in Semiconductors, Optoelectronics and Nanostructures (EDISON 17), August 7-12, 2011, Santa Barbara, California, USA, pp. 50-51.
12. V. Ryzhii, M. Ryzhii, A. Dubinov, V. Aleshkin, V. Mitin, M. Shur, A. Satou, S. A. B. Tombet and T. Otsuji, “Concepts of Terahertz and Infrared Devices Based on Graphene Structures,” invited talk at Proceedings of the 36th International Conference on Infrared, Millimeter and Terahertz Waves (IRMMW), October 2-7, 2011, Houston, Texas, USA, Proceedings Tu3C.1.
13. V. Mitin, “High Performance Solar Cells and Photodetectors on Quantum Dot Structures with Built-in-Charge,” invited talk at the BIT's 1st Annual World Congress of Nano-S & T, October 23-26, 2011, Dalian, China.
14. N. Vagidov, A. Sergeev, A. Antipov, K. Sablon, J. Little, and V. Mitin,“Quantum-Dot Nanostructures for Effective Harvesting, Detection, and Conversion of IR Radiation,” APS March Meeting, February 27 – March 2, 2012, Boston, Massachusetts, book of abstracts A33.11.
15. F. Vasko, V. Mitin, and A. Sergeev, “Effects of Disorder on Recombination and Relaxation Processes via Acoustic Phonons in Graphene,” APS March Meeting, February 27 – March 2, 2012, Boston, Massachusetts, book of abstracts D11.10.
16. V. Mitin and F. Vasko, “Superlattice Formed by Quantum Dot Sheets: Density of States and IR Absorption,” APS March Meeting, February 27 – March 2, 2012, Boston, Massachusetts, book of abstracts S1.149.

17. J. K. Choi, N. Vagidov, A. Sergeev, G. Strasser, F. Vasko, and V. Mitin, “Voltage-Tunable IR Photodetector Based on Asymmetrically Doped Coupled Quantum Wells”, APS March Meeting, February 27 – March 2, 2012, Boston, Massachusetts, book of abstracts S1.150.
18. F.T. Vasko and V. Mitin, “Generation-Recombination Processes via Acoustic Phonons and Transient Population Inversion in Graphene,” invited talk at the Japan-Russia-USA Symposium on Modeling of Graphene Terahertz, Nano-Mechanical, and Acousto-Optical Devices, Aizu-Wakamatsu, Japan, March 7-10, 2012, book of abstracts.
19. V. Mitin and F. Vasko, “Superlattice Formed by Quantum Dot Sheets: Density of States and IR Absorption”, NANOSMAT-USA International Conference on Surfaces, Coatings, and Nano-Structured Materials, March 27-30, 2012, Tampa, FL.
20. V. Mitin and F. Vasko, “Nonequilibrium Carriers in Graphene: Diffusion, Recombination, and Transient Population Inversion,” invited talk at the US-Japan TeraNano Workshop on Nanophotonics and Nanoelectronics, May 11, 2012, Buffalo, NY.
21. V. Ryzhii, N. Ryabova, M. Ryzhii, T. Otsuji, V. Mitin, and V.E. Karasik, “Concept of Terahertz and Infrared Detectors Based on Graphene Strusctures,” Quantum Structure Infrared Photodetector International Conference, QSIP 2012, June 17-23, 2012, Cargese, Corsica, France, Book of abstracts p. 33, and the Proceedings of the International Conferenece on Quantum Structure Infrared Photodetector International Conference (QSIP) 2012, editors Ph. Bois and S.D. Gunapala, Elsevier, pp. 137-141.
22. S. Oktyabrsky, V.E. Tokranov, M. Yakimov, A.V. Sergeev, Vladimir V. Mitin, “Nanoengineered quantum dot medium for space optoelectronic devices,”, Keynote Presentation, Paper 8519-6 at the SPIE Optical Engineering + Applications, 12 - 16 August 2012. San Diego, CA and paper in SPIE Optics + Photonics Proc. SPIE 8519, 851907 (2012).
23. A. Sergeev, N. Vagidov, V. Mitin, K. Sablon, and J. Little, “Nanoscale engineering of photoelectron processes by charging quantum dots”, IEEE NANO 2012, 12th International Conference on Nanotechnology, 20 - 23 August 2012, Birmingham, UK, book of abstracts.
24. V. Mitin, A. Sergeev, N. Vagidov, K. Sablon, M. Yakimov, and S. Oktyabrsky, “Photoelectron Kinetics in Nanomaterials with Charged Dots: Physics and Applications”, Invited talk at the 7th International Cnference on Surfaces, Coatings and Nanostructured Materials (Nanosmat), 18-21 September 2012, Prague, Technical Program, p.14, Talk Nano-108.
25. V. Ryzhii, T. Otsuji, M. Ryzhii, V. Mitin, M.S. Shur, “Graphene-based infrared and terahertz detectors: Concepts, features, and comparison,” invited talk at Int. Conf. on Micro and Nanoelectronics (ICMNE), L2-01, Moscow, Russia, Oct. 1-5, 2012.
26. V. Mitin, F. T. Vasko, V. Ryzhii, and T. Otsuji, “Interplay of Intraband and Interband Absorption in a Disordered Graphene,” 3rd International Sympposium on Graphene Devices (ISGD-2012), November 5-9, 2012, Synchrotron SOLEIL, Saint-Aubin, France, book of abstracts, OC-05, p. 16.
27. “V. Mitin, K. Sablon, J. Little, A. Sergeev, and N. Vagidov, “Nanomaterials with Charged Quantum Dots for Conversion and Sensing Applications,” invited talk at 2012 MRS Fall Meeting, November 25-30, 2012, Boston, MA, Talk E8.03*, p. 160 of the Program.
28. V. Mitin, F. T. Vasko, V. Ryzhii, and T. Otsuji, “Distinctiveness of Non-equilibrium Carriers in Disordered Graphene,” 3rd International Simposium on Terahertz Nanoscience, December 10-12, 2012, Honolulu, Hawaii, book of abstracts, p. 20.
29. A. Satou, V. Ryzhii, F.T. Vasko, V.V. Mitin, T. Otsuji, “Numerical simulation of terahertz plasmons in gated graphene structures,” SPIE Photonics West, 8624-37, San Francisco, CA, Feb. 6, 2013, book of abstracts.
30. G. Thomain, V. Mitin, V.Pogrebnyak, and A. Sergeev, “Effect of doping on performance of IR quantum dot photodetector,” APS March Meeting 2013, March 18–22, 2013; Baltimore, Maryland, book of abstracts.
31. A. Sergeev, M. Reizer, and V. Mitin, “Electron relaxation via interaction with optical phonons in disordered metals and semiconductors,” APS March Meeting, March 18–22, 2013; Baltimore, Maryland.
32. V. Ryzhii, T. Otsuji, M. Ryzhii, V. Mitin and M.S. Shur, “Terahertz detectors and photomixers based on double-graphene-layer structures utilizing plasma resonances,” International Workshop on Optical Terahertz Science and Technology 2013, Kyoto, Japan, April 1-5, 2013, book of abstracts TH3-04.
33. V. Mitin, N. Vagidov, K. Sablon, and A. Sergeev, “Adaptive quantum-dot based materials for detection and broad band photovoltaic conversion,” invited talk at the SPIE Defense, Security and Sensing 2013,

April 28-May 3, 2013, Baltimore, MD.
34. V. Mitin, G. Thomain, N. Vagidov, A. Sergeev, M. Yakimov, and S. Oktyabrsky, “Adaptable quantum dot nanomaterials for advanced sensing,”, International Conference on Materials and Applications for Sensors and Transducers (IC-MAST 2013), Prague, Czech Republic, September 13-17, 2013.
35. V. Mitin, A. Sergeev, N. Vagidov, and K. Sablon, “Nanomaterials with charged quantum dots for broad band solar energy conversion and advanced sensing,” Nano and Giga Challenges in Electronics, Photonics and Renewable Energy: From Materials to Devices to System Architecture, Symposium and Spring School, Phoenix, Arizona, March 10-14, 2014.
36. V. Mitin, V. Ryzhii, T. Otsuji, V. Ya. Aleshkin, A. A. Dubinov, M. Ryzhii, and M. S. Shur, “High sensitivity terahertz and infrared detectors based on double-graphene-layer structures,” International Conference on Materials and Applications for Sensors and Transducers (IC-MAST 2014), Bilbao, Spain, June 8-11, 2014, book of abstracts.
37. “Nanomaterials with manageable charge of nanoblocks for adaptive sensing”, APS March Meeting 2014, March 3–7, 2014; Denver, CO, book of abstracts.
38. G. Thomain, X. Zhang, N. Vagidov, V. Mitin, and A. Sergeev, “Challenges in quantum dot IR/THz sensing technologies,” The 3rd RJUS Symposium on Fundamental & Applied Problems of Terahertz Devices & Technologies, June 17-20, 2014, University at Buffalo, NY, USA.
39. A. Sergeev, V. Mitin, N. Vagidov, K. Sablon, J. Little, K. Reinhardt, “Adaptable quantum dot nanomaterials with controllable kinetics,” International Conference on Physics of Semiconductors, ICPS 2014, August 10-15, Austin, TX, USA.
40. T. Otsuji, V. Ryzhii, S. Boubanga Tombet, T. Watanabe, A. Satou, M. Ryzhii, A. Dubinov, V. Ya Aleshkin, V. Popov, V. Mitin, and M.S. Shur, “Graphene plasmonic heterostructures for new typse of terahertz lasers”, SPIE Optics + Photonics 2014, Conf. 9199, Terahertz Emission, Detection and Applications V, 9199-14, San Diego, CA, USA, 17 Aug. 2014. (invited); Proc. SPIE, Vol. 9199, pp. 91990F-1-10
41. T. Otsuji, T. Watanabe, A. Satou, S. A. Boubanga-Tombet, A. Dubinov, V. V. Popov, V. Mitin, V. Ryzhii, “Giant Terahertz Gain by Excitation of Surface Plasmon Polaritons in Optically Pumped Graphene”, ISGD: 4th International Symposium on Graphene Devices, A4.05, Seattle, USA, 25 Sept. 2014. (invited)
42. A. Sergeev and V. Mitin, “Nanoscale Engineering of Energy Transfer in Optoelectronic Materials for Sensing and Conversion,” invited talk at Functional Materials Division, Materials and Manufacturing Directorate of AFOSR, Dayton, October 28, 2014.
43. X. Zhang, A. Sergeev. V. Mitin, K. Sablon, M. Yakimov, and S. Oktyabrsky, “Adaptable Quantum Dot Nanomaterials for IR Sensing”, APS March Meeting 2015, March 2-6, 2015; San Antonio, Texas, Bulletin of the American Physical Society, V. 60, No. 1, V1.00198.
44. V. Mitin, A. Sergeev, X. Zhang, and T. Yore, “Reconfigurable nanomaterials for adaptive sensing: Electric and optical control of nanoscale potential profile”, Advanced Research Workshop "Future Trends in Microelectronics: Journey into the Unknown", June 21-26, 2015 Mallorca, Spain, book of abstract, paper to be published in proceedings.

Thesis/Dissertations
1. G. Thomain, “Nanoscale engineering of photoelectron processes for infrared detection,” Ph.D. Dissertation, July 2014, State University of New York at Buffalo, ProQuest, UMI Dissertations Publishing, 2014. 3640883

Changes in research objectives (if any):

none

Change in AFOSR Program Manager, if any:

Started with Dr. Kitt Reinhardt
Currently: Dr. Kenneth C. Goretta

Extensions granted or milestones slipped, if any:

None

AFOSR LRIR Number

LRIR Title

Reporting Period

Laboratory Task Manager

Program Officer

Research Objectives

Technical Summary

Funding Summary by Cost Category (by FY, $K)

	Starting FY	FY+1	FY+2
Salary			
Equipment/Facilities			
Supplies			
Total			

Report Document

Report Document - Text Analysis

Report Document - Text Analysis

Appendix Documents

2. Thank You

E-mail user

Oct 24, 2015 16:49:27 Success: Email Sent to: vmitin@buffalo.edu